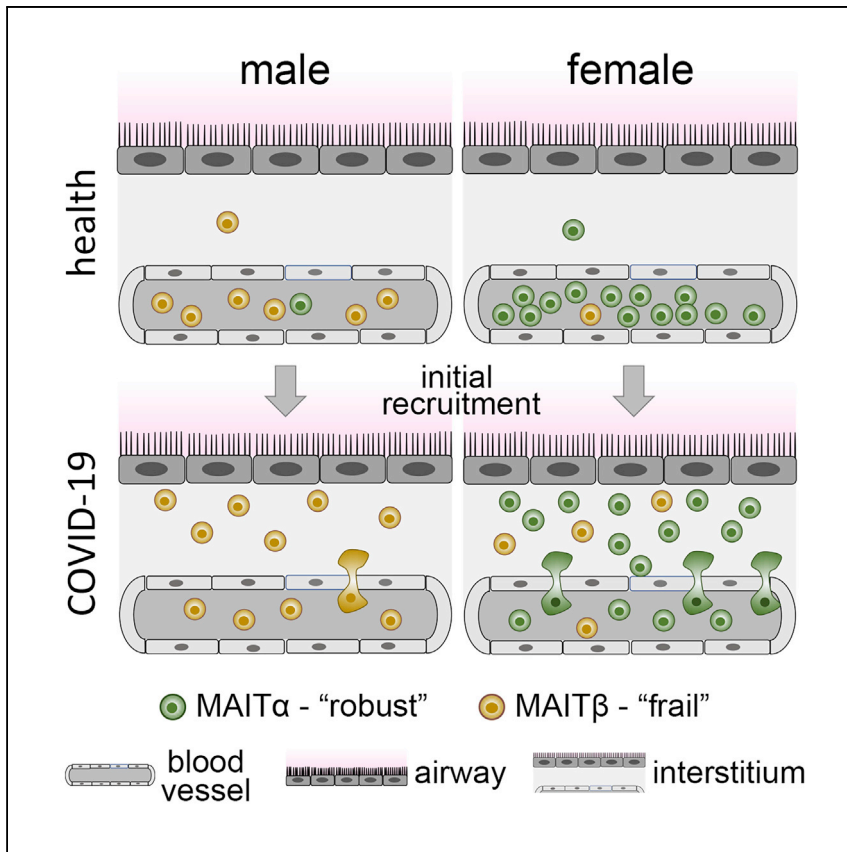# Med

Clinical and Translational Article

Mucosal-associated invariant T cell responses differ by sex in COVID-19

Responses in COVID-19 patients are distinct across sexes. Yu et al. show that, compared with male patients, female COVID-19 patients exhibit evidence of a major recruitment wave of circulating mucosal-associated invariant T (MAIT) cells into the airways and demonstrate that these cells display an immunologically active phenotype.

Translation to Patients

Chen Yu, Sejiro Littleton, Nicholas S. Giroux, ..., Christopher W. Woods, Xiling Shen, Daniel R. Saban

xiling.shen@duke.edu (X.S.)
daniel.saban@duke.edu (D.R.S.)

Highlights

Circulating MAIT cell frequencies were associated negatively with COVID-19 severity

This pattern was driven by a pronounced reduction of circulating MAIT cells in females

MAIT cell gene profile was immunologically active in females but pro-apoptotic in males

Frequency and phenotype of MAIT cells in airway samples were superior in females

CellPress

Clinical and Translational Article

Mucosal-associated invariant T cell responses differ by sex in COVID-19

Chen Yu,[1,11] Sejiro Littleton,[1,2,11] Nicholas S. Giroux,[3] Rose Mathew,[1] Shengli Ding,[3] Joan Kalnitsky,[1] Yuchen Yang,[4,5] Elizabeth Petzold,[6] Hong A. Chung,[3] Grecia O. Rivera,[3] Tomer Rotstein,[3] Rui Xi,[3] Emily R. Ko,[6,7] Ephraim L. Tsalik,[6,8,9] Gregory D. Sempowski,[10] Thomas N. Denny,[10] Thomas W. Burke,[6] Micah T. McClain,[6,8,9] Christopher W. Woods,[6,8,9,10] Xiling Shen,[3,*] and Daniel R. Saban[1,2,12,*]

SUMMARY

Background: Sexual dimorphisms in immune responses contribute to coronavirus disease 2019 (COVID-19) outcomes, but the mechanisms governing this disparity remain incompletely understood.

Methods: We carried out sex-balanced sampling of peripheral blood mononuclear cells from hospitalized and non-hospitalized individuals with confirmed COVID-19, uninfected close contacts, and healthy control individuals for 36-color flow cytometry and single-cell RNA sequencing.

Findings: Our results revealed a pronounced reduction of circulating mucosal-associated invariant T (MAIT) cells in infected females. Integration of published COVID-19 airway tissue datasets suggests that this reduction represented a major wave of MAIT cell extravasation during early infection in females. Moreover, MAIT cells from females possessed an immunologically active gene signature, whereas cells from males were pro-apoptotic.

Conclusions: Our findings uncover a female-specific protective MAIT cell profile, potentially shedding light on reduced COVID-19 susceptibility in females.

Funding: This work was supported by NIH/NIAID (U01AI066569 and UM1AI104681), the Defense Advanced Projects Agency (DARPA; N66001-09-C-2082 and HR0011-17-2-0069), the Veterans Affairs Health System, and Virology Quality Assurance (VQA; 75N93019C00015). The content is solely the responsibility of the authors and does not necessarily represent the official view of the National Institutes of Health. COVID-19 samples were processed under Biosafety level 2 (BSL-2) with aerosol management enhancement or BSL-3 in the Duke Regional Biocontainment Laboratory, which received partial support for construction from NIH/NIAID (UC6AI058607).

INTRODUCTION

Severe acute respiratory syndrome coronavirus 2 (SARS-CoV-2) has led to a global pandemic of coronavirus disease 2019 (COVID-19) and a death toll of more than 2.3 million people and rising.[1] According to reported sex-disaggregated data, males are affected disproportionately by SARS-CoV-2, with a higher incidence of cases, mortality, and morbidity.[2] This follows a similar trend of higher case fatality rates for males in SARS-CoV and Middle East respiratory syndrome CoV (MERS-CoV) and experiments using SARS-CoV mouse models.[2–6] Sex differences in the immune response are thought to be a key contributing factor to these CoV disease

Context and significance

Why are women twice as less likely than men to experience severe COVID-19? Answering this question may help us more completely understand the immune defenses that counter SARS-CoV-2. This study from researchers at Duke University suggests that a type of white blood cells, mucosal-associated invariant T (MAIT) cells, is superior in women with COVID-19. The potential importance of the finding is that these highly specialized white blood cells have been shown to contribute critically to immune defenses in other viral and bacterial infections. These findings may shed light on the underlying reasons for reduced COVID-19 susceptibility in women and highlights the potential role of MAIT cells in countering SARS-CoV-2.

outcomes, agreeing with the current body of knowledge indicating that innate and adaptive immune responses are altered substantially according to sex.[7–10] Specific to SARS-CoV-2 infection, responses of lymphocytes and myeloid cells have been shown to be associated with COVID-19 outcomes.[11–19] Correspondingly, a recent study of sex differences in COVID-19 immune responses uncovered an association between poor disease outcomes in males and weak T cell responses in CD4+ and CD8+ compartments, whereas poor outcomes in females were associated with high innate immune cytokines, tumor necrosis factor superfamily 10 (TNFSF-10), and interleukin-15 (IL-15).[20] The sex differences elucidated in this seminal study further cement the need to better understand the mechanisms governing sex-specific susceptibility to SARS-CoV-2.

RESULTS

In this study, we carried out sex-balanced sampling of peripheral blood mononuclear cells (PBMCs) from individuals with COVID-19 and control subjects for 36-color flow cytometry and single-cell RNA sequencing (scRNA-seq) analyses. A total of 88 samples were analyzed from 45 individuals. Details regarding subject demographics and sample information are summarized in Figure 1A and Tables 1 and S1). Briefly, we analyzed samples from 28 individuals with COVID-19 as confirmed by positive SARS-CoV-2 PCR and/or immunoglobulin G (IgG) seroconversion. These included 9 hospitalized subjects (20%), 7 requiring intensive care, hereafter referred to as "hospitalized." An additional 19 subjects were identified in non-hospital settings (42.2%), hereafter referred to as "infected." Most of these confirmed COVID-19 cases were sampled longitudinally (range, 1–28 days), including pre- and post-anti-SARS-CoV-2 IgG seroconversion. The dates of symptom onset for all subjects with confirmed COVID-19 were recorded at enrollment, providing an illness range of 1–40 days. We also recorded symptom severity, obtained via investigator survey on 39 symptoms related to COVID-19 (STAR Methods). Additionally, we included 7 subjects (15.6%), hereafter referred to as "exposed," who were also sampled at multiple time points. These subjects, despite being close contacts of infected individuals, remained with negligible symptom scores, were negative for SARS-CoV-2 by PCR, and did not demonstrate detectable anti-SARS-CoV-2 IgG for at least 2 months after enrollment. Last, we included a group of 10 "healthy" subjects (22.2%) who were enrolled prior to the pandemic in 2019 and did not show any symptoms associated with COVID-19 or other respiratory illness.[21]

Immune profiling of PBMCs from individuals with COVID-19 reveals the association of CD8+CD161hi T cell frequencies with disease severity

With these flow cytometry data, we generated a map of immune cell populations and their subsets by down-sampling to 3,000 viable CD45+ singlets per sample and concatenated all data for uniform manifold approximation and projection (UMAP)[22] and unbiased clustering via flow self-organizing maps (FlowSOM).[23] Unique marker expression of respective populations facilitated our annotation of major PBMC populations (Figures 1B and 1C), including CD4+ and CD8+ (αβ) T cells, γδ T cells, B cells, plasmablasts, natural killer (NK) cells, monocytes (MOs), and dendritic cells (DC), which were also confirmed by manual analysis (Figures S1A–S1H). Subpopulations were also annotated in this manner, such as CD45RA+ CD27+ CCR7+ naive, CD45RA− CCR7+ central memory (CM), CD45RA− CCR7− effector memory (EM), and CD45RA+ CD27− CCR7− terminally differentiated EM (terminally differentiated effector memory cells re-expressing CD45RA [EMRA]) CD8+ T cells and CD8+ CD161hi T cells and other indicated subpopulations (Figures 1B, 1C, and S1A–S1H). We noted that a minor population of basophils (Basos) and

[1]Department of Ophthalmology, Duke University School of Medicine, Durham, NC 27710, USA

[2]Department of Immunology, Duke University School of Medicine, Durham, NC 27710, USA

[3]Department of Biomedical Engineering, Pratt School of Engineering, Duke University, Durham, NC 27710, USA

[4]Department of Pathology and Laboratory Medicine, University of North Carolina at Chapel Hill, Chapel Hill, NC 27599, USA

[5]McAllister Heart Institute, University of North Carolina at Chapel Hill, Chapel Hill, NC 27599, USA

[6]Center for Applied Genomics and Precision Medicine, Duke University, Durham, NC 27710, USA

[7]Duke Department of Medicine, Duke University School of Medicine, Durham, NC 27710, USA

[8]Durham Veterans Affairs Health Care System, Durham, NC 27705, USA

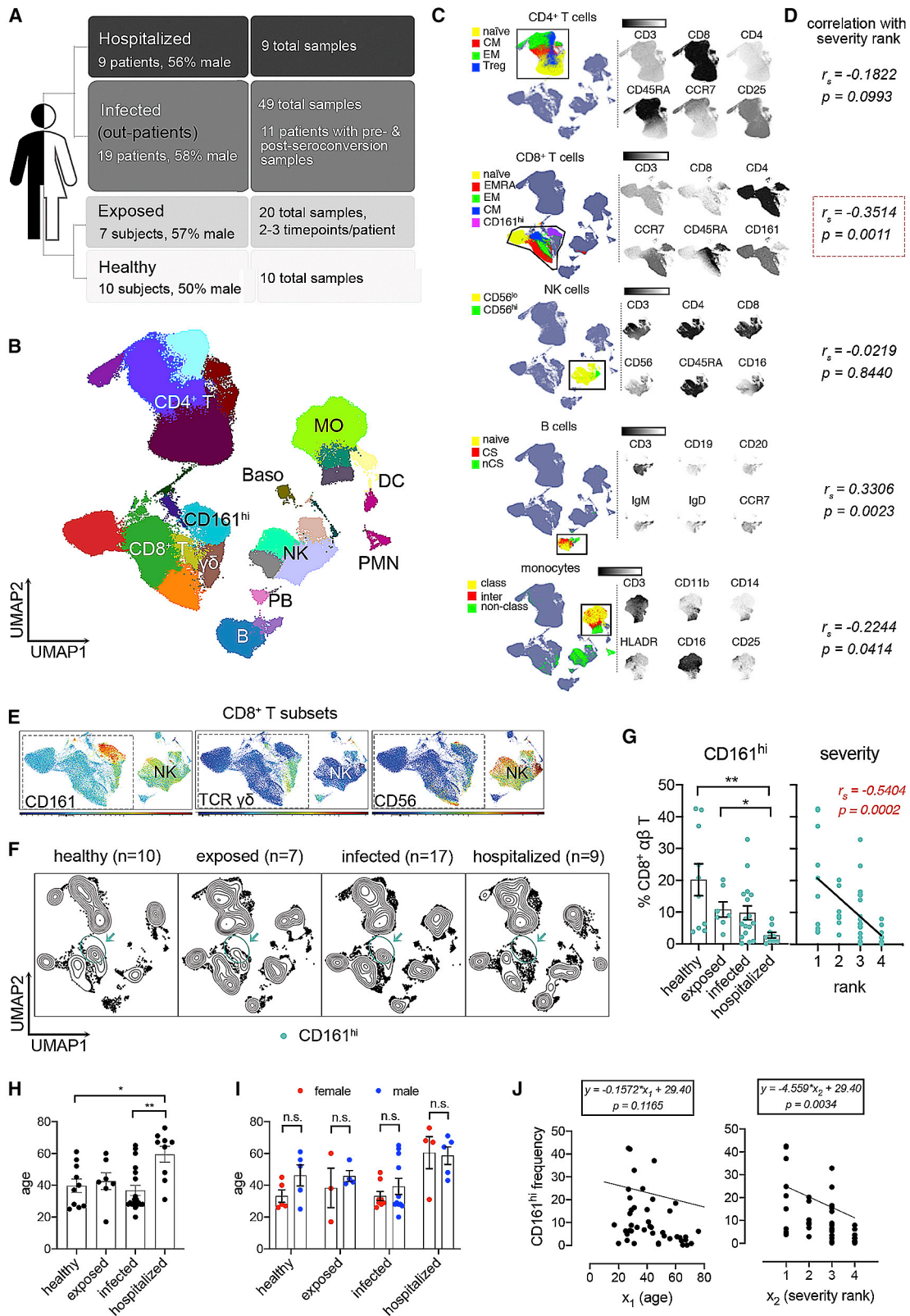[9]Division of Infectious Diseases, Duke University Medical Center, Durham, NC 27710, USA

[10]Duke Human Vaccine Institute, Duke University Medical Center, Durham, NC 27710, USA

[11]These authors contributed equally

[12]Lead contact

*Correspondence: xiling.shen@duke.edu (X.S.), daniel.saban@duke.edu (D.R.S.)

A

Hospitalized
9 patients, 56% male — 9 total samples

Infected (out-patients)
19 patients, 58% male — 49 total samples
11 patients with pre- & post-seroconversion samples

Exposed
7 subjects, 57% male — 20 total samples, 2-3 timepoints/patient

Healthy
10 subjects, 50% male — 10 total samples

B

C

D correlation with severity rank

CD4+ T cells — naïve, CM, EM, Treg

CD3, CD8, CD4, CD45RA, CCR7, CD25

$r_s = -0.1822$
$p = 0.0993$

CD8+ T cells — naïve, EMRA, EM, CM, CD161hi

CD3, CD8, CD4, CCR7, CD45RA, CD161

$r_s = -0.3514$
$p = 0.0011$

NK cells — CD56lo, CD56hi

CD3, CD4, CD8, CD56, CD45RA, CD16

$r_s = -0.0219$
$p = 0.8440$

B cells — naïve, CS, nCS

CD3, CD19, CD20, IgM, IgD, CCR7

$r_s = 0.3306$
$p = 0.0023$

monocytes — class, inter, non-class

CD3, CD11b, CD14, HLADR, CD16, CD25

$r_s = -0.2244$
$p = 0.0414$

E CD8+ T subsets

CD161, TCR γδ, CD56, NK

F

healthy (n=10), exposed (n=7), infected (n=17), hospitalized (n=9)

● CD161hi

G

CD161hi   severity

% CD8+ αβ T

healthy, exposed, infected, hospitalized

rank

$r_s = -0.5404$
$p = 0.0002$

H

age

healthy, exposed, infected, hospitalized

I

● female ● male

age

healthy, exposed, infected, hospitalized

J

$y = -0.1572 \cdot x_1 + 29.40$
$p = 0.1165$

CD161hi frequency

x_1 (age)

$y = -4.559 \cdot x_2 + 29.40$
$p = 0.0034$

x_2 (severity rank)

neutrophils (polymorphonuclear neutrophils [PMNs]), primarily from hospitalized individuals, were detected (Figure 1B) despite using a PBMC isolation protocol.

We next set out to screen our flow cytometry dataset for immune populations that exhibited major quantitative changes associated with COVID-19 severity. Regression analysis revealed a significant ($p < 0.05$) association of several major PBMC populations, including CD8^{+} T cells, NK cells, B cells, and MOs relative to disease severity rank (i.e., healthy, exposed, infected, and hospitalized) (Figure 1D). The highest degree of association with the most significance was found in CD8^{+} T cells (Figure 1D). Additional analysis of CD8^{+} T subpopulations also revealed significant changes in CD8^{+} EM T cells (Figure S1I) and in CD8^{+} CD161^{hi} T cells with high significance ($p = 0.0006$) (Figure S1I). Other significant changes were also observed, such as in B cell subpopulations (naive, IgD^{+} non-class switch, and plasmablasts), NK cells (CD56^{lo} populations), DCs (CD11c^{+} DCs and plasmacytoid DCs [pDCs]), MOs (classical, intermediate, and nonclassical). and CD4^{+} (EM) αβ T cells (Figure S1I). Our findings therefore suggest that the frequencies of certain lymphocyte and myeloid populations are affected in COVID-19, including a major effect on CD8^{+} CD161^{hi} (αβ) T cells.

The robust statistical changes in total CD8^{+} T cells and the CD8^{+} CD161^{hi} T subpopulation prompted us to look at these cells more closely. Regarding annotation of this CD161^{hi} cluster, because the overwhelming majority of events were low to negative for CD56 and for T cell receptor γδ (TCRγδ) (Figure 1E), the phenotype was largely consistent with mucosal-associated invariant T (MAIT) cells but not NK T or γδ T cells. This designation is congruent with recent work with COVID-19 PBMCs.[24–27] Next we performed a more focused analysis of this cluster in COVID-19 by assessing their frequencies by severity rank using samples taken within 3 days of enrollment, the time point most proximal to the initial symptom score recordings. Results were displayed via UMAP contour plots, revealing a reduction in these cells in the SARS-CoV-2 settings (Figure 1F). Manual gating (CD3^{+} TCRγδ^{−} CD8^{+} CD161^{hi}) from all flow cytometry events revealed a significant reduction when comparing healthy ($p = 0.0036$) or exposed ($p = 0.0488$) subjects versus hospitalized subjects and a negative correlation ($p = 0.0002$) with disease severity rank (Figure 1G). Moreover, the ages of the hospitalized group are significantly higher than those of other groups (Figure 1H), although the ages of sampled subjects were similar between sexes at each severity rank (Figure 1I). To address the potential confounding factor of age, we built a multiple regression model with age and severity rank as two independent variables (Figure 1J). Our results showed that age does not significantly ($p = 0.1165$) affect CD161^{hi} cells but severity rank does ($p = 0.0034$). Therefore, we concluded that changes of these CD161^{hi} cells are associated with COVID-19 disease severity.

Figure 1. Loss of peripheral CD8^{+}CD161^{hi} T cell frequencies correlates with increased severity of COVID-19

(A) Overview of groups in this study.

(B) UMAP visualization of PBMC subsets identified by FlowSOM clustering. Samples from all participants were pooled and down-sampled to 3,000 live CD45^{+} cells per sample. MO, monocyte; NK, natural killer; DC, dendritic cell; PMN, polymorphonuclear neutrophil; Baso, basophil.

(C) Representative marker expression by CD4^{+} T cell, CD8^{+} T cell, MO, NK cell, and B cell subsets.

(D) Correlation analysis of immune cell subsets as shown in (C) with disease severity rank.

(E) Expression of CD161, TCR γδ and CD56 in CD8^{+} T cell subsets. NK cells were used as a positive control for CD56 expression.

(F) UMAP of samples grouped by disease severity rank. Samples collected within 3 days from initial symptom score recording were included.

(G) Frequencies of CD161^{hi} T cells (mean ± standard error) in different severity groups (left) and their correlation with severity rank (right).

(H and I) Age comparisons among severity rank and between sexes.

(J) Multiple linear regression of age (x_1) and severity rank (x_2) with CD161^{hi} cell frequencies. Regression models with p values are shown for age and severity rank.

Significance was determined by Kruskal-Wallis test with Dunn's test (E) or ANOVA (H and I): *$p < 0.05$, **$p < 0.01$, ***$p < 0.001$. Correlation efficiency was calculated by Spearman's rank correlation (D and G). See also Figure S1 and Tables 1 and S1.

Table 1. Summary of demographics and sample information

Group		Healthy	Exposed	Infected	Hospitalized	Total
Age (mean ± SD [range])		39.70 ± 13.68 (25–61)	42.57 ± 13.93 (17–60)	36.73 ± 13.88 (20–65)	59.44 ± 15.11 (31–76)	42.84 ± 16.06 (17–76)
Number of subjects (female:male [F:M] ratio)		n = 10 (5:5)	n = 7 (3:4)	n = 19 (8:11)	n = 9 (4:5)	n = 45 (20:25)
Race (n [%])	African American	3 (30.00%)	0	1 (5.26%)	5 (55.56%)	9 (20.00%)
	Asian	0	1 (14.29%)	2 (10.53%)	0	3 (6.67%)
	White	7 (70.00%)	5 (71.42%)	16 (84.21%)	3 (33.33%)	31 (68.89%)
	Others/ unknown	0	1 (14.29%)	0	1 (11.11%)	2 (4.44%)
Days since onset when enrolled (mean ± SD [range])		N/A	15.17 ± 11.25 (5–33)	11.18 ± 4.30 (3–19)	8.25 ± 6.14 (1–18)	11.19 ± 6.73 (1–33)
# samples of flow cytometry (F:M ratio)		n = 10 (5:5)	n = 20 (9:11)	n = 44 (21:23)	n = 9 (4:5)	n = 83 (39:44)
# samples of scRNA-seq (F:M ratio)		n = 5 (3:2)	n = 8 (3:5)	n = 29 (12:17)	n = 6 (1:5)	n = 48 (19:29)
Days since onset when samples collected mean ± SD (range)		N/A	26.94 ± 14.94 (5–61)	18.27 ± 8.44 (3–40)	8.25 ± 6.14 (1–18)	19.32 ± 11.44 (1–61)

See also Table S1.

Elucidation of sex differences in CD8^{+} lymphocytes during SARS-CoV-2 infection

Given the previously reported sex differences in immune responses in COVID-19,[2,20] we further grouped the data by sex and characterized the frequencies of CD8^{+} subsets stratified by disease severity rank (Figures 2A, 2B, S2A, and S2B), time after symptom onset (early, ≤14 days; middle, 15–21 days; late, >21 days) (Figures 2C–2E), and seroconversion status (Figure 2F). The severity rank results showed that healthy females had greater frequencies of CD161^{hi} cells relative to males and that females had a more dramatic loss of peripheral CD161^{hi} cells compared with males in COVID-19 (Figures 2A–2C). We also found that, within the CD8^{+} compartments of healthy subjects, males had greater frequencies of CD8^{+} memory T cells (combined EMRA, EM, and CM) (Figures 2D and 2E). Although the memory cell predominance in males was preserved at all time points, the greater abundance of CD161^{hi} cells in females was lost at early and middle time points but not in late disease (Figures 2D and 2E). The loss of this difference was due to a precipitous drop of CD161^{hi} cells in females at early and middle time points (Figure 2F). No obvious changes of naive CD8^{+} T cells were found (Figure S2C). Last, when analyzing data from individuals with confirmed COVID-19 by seroconversion status, we found that CD161^{hi} cells were higher in females relative to males prior to seroconversion, whereas CD8^{+} memory cells were higher in males in seroconverted subjects (Figure 2G). We identified a female-specific decline in circulating CD161^{hi} cell frequencies upon exposure to/infection with SARS-CoV-2. This sex-specific reduction may be due to extravasation into airway tissue, suggesting a sex-specific role of these CD161^{hi} cells in COVID-19.

scRNA-seq uncovers the role of CD161^{hi} T lymphocytes in SARS-CoV-2 immune responses

Next we analyzed scRNA-seq (10x Genomics) data of 48 different PBMC samples from 24 subjects across all groups (Tables 1 and S1) to further characterize these
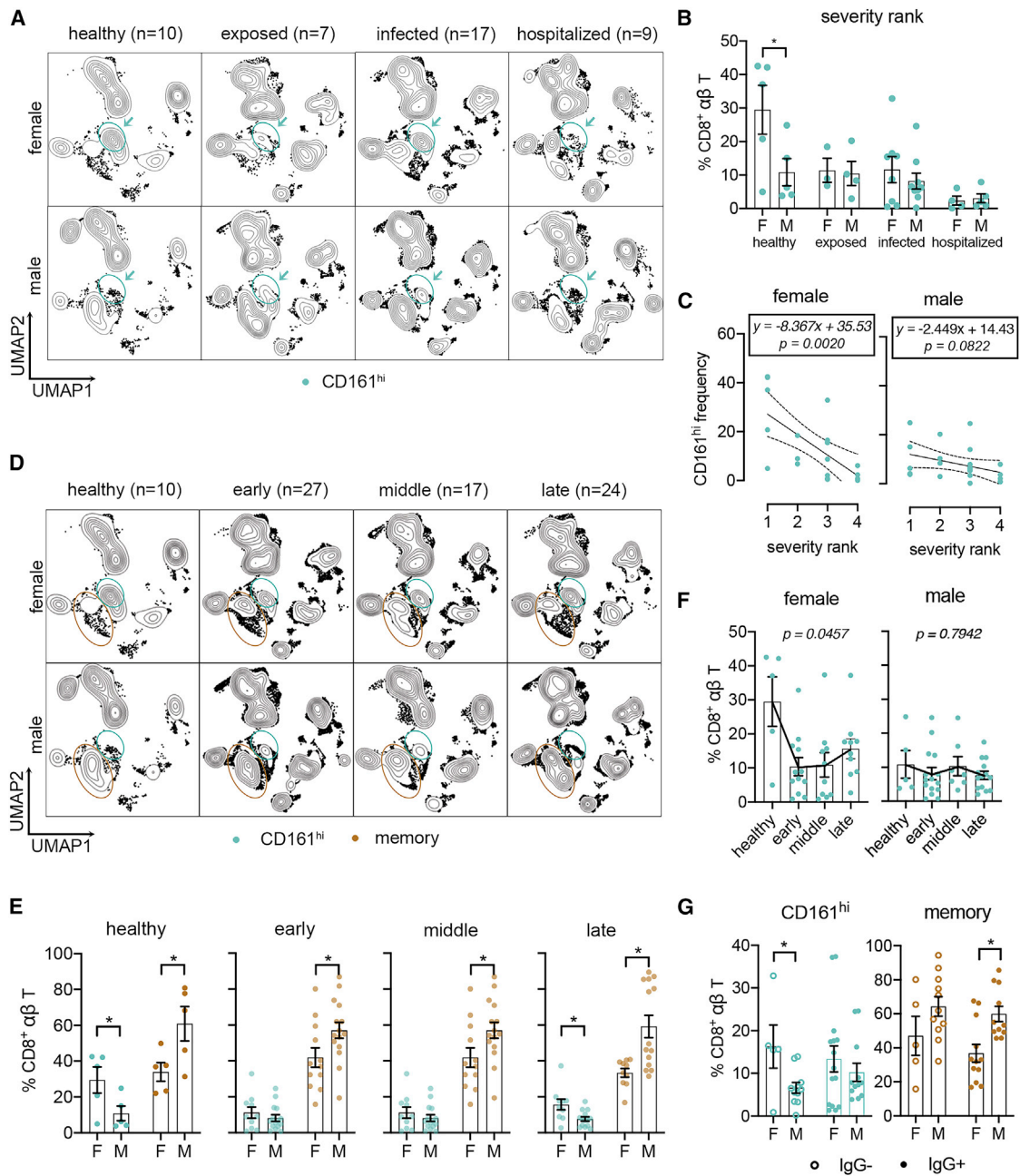
Figure 2. Sex-specific responses of circulating CD8$^+$ T cells in individuals with COVID-19

(A) UMAP of samples stratified by sex and severity rank as shown in Figure 1F.

(B) Frequencies of CD161^{hi} cells between females and males at each rank group.

(C) Linear regression of CD161^{hi} cells with severity rank between sexes. Dashed lines indicate 95% confidence intervals. Regression models with p values are shown for each sex.

(D) UMAP of samples stratified by sex and time after symptom onset (early, ≤14 days; middle, >15 days and ≤21 days; late, >22 days).

(E) Frequencies of CD161^{hi} and memory CD8$^+$ T cells between sexes and time points.

(F) Sex-specific changes of CD161^{hi} cells frequencies shown in (E).

(G) Frequencies of CD161^{hi} and memory CD8$^+$ T cells in samples from subjects with confirmed COVID-19 pre- and post-seroconversion.

Data were plotted as mean ± standard error (B and E–G). Significance was determined by Mann-Whitney test (B, E, and G) and Kruskal-Wallis test with Dunn's test (F): *p < 0.05. See also Figure S2.
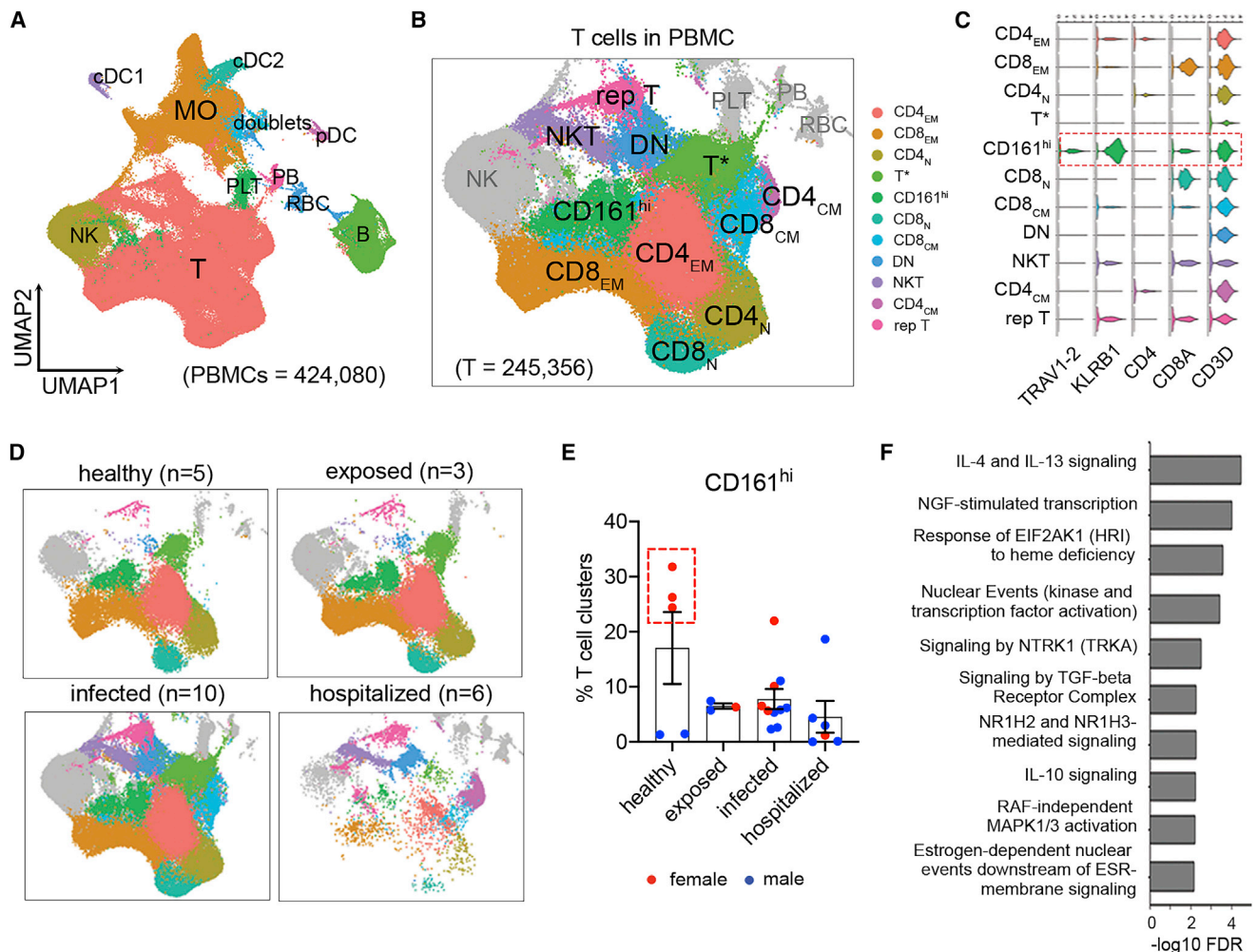
Figure 3. Characterization of CD8⁺CD161ʰⁱ T cells among COVID-19 PBMCs using scRNA-seq

(A) UMAP and unsupervised cluster analysis of PBMCs. RBC, red blood cell; PB, plasmablast; PLT, platelet.

(B and C) Visualization of T cell subsets with high resolution in UMAP (B) and expression of their marker genes as indicated in violin plots (C). The T* cluster likely represents a dropout population with low unique molecular identifier (UMI) counts. N, naive; EM, effector memory; CM, central memory; DN, double negative; rep, replicating.

(D) Changes of T cell subsets with severity rank. N, number of individuals.

(E) Frequencies of CD161ʰⁱ clusters relative to all T cell subsets. Females were plotted in red and males in blue. The red dashed box delineates healthy females.

(F) Top enriched pathways of CD161ʰⁱ clusters in the Reactome Pathway Database, ranked by false discovery rate (FDR; −log10 scale).

Data were plotted as mean ± standard error. Significance was determined by Kruskal-Wallis test (E). See also Figure S3 and Table S2.

CD161ʰⁱ cells. Data were processed using the Seurat 3 package,[28] and subsequent transcript-based annotation was carried out (Figures 3A, S3A, and S3B). Within T cell subsets (Figure 3B; Table S2), we were able to identify CD161ʰⁱ cells in a single cluster containing high *KLRB1* (i.e., CD161) expression and co-expression of *CD3D*, *CD8A*, and *TRAV1-2* (Figures 3C and S3B), which encodes the Vα7.2 invariant TCR α chain on MAIT cells. Grouping these data by disease severity showed that hospitalized individuals had lower frequencies of T cells, including CD161ʰⁱ cells (Figure 3D), agreeing with our flow cytometry findings and consistent with reported lymphopenia in individuals with severe COVID-19.[11,20,29–32] Also showing the same trend as our flow cytometry data was the higher frequency of CD161ʰⁱ cells in healthy adults (Figure 3E), although it did not reach statistical significance because of the

variations between females and males. Next, to address the functional role of this CD161^{hi} cluster in COVID-19, we performed gene enrichment analysis using differentially expressed genes (DEGs) calculated by comparing the CD161^{hi} cluster from all samples with all other T cell clusters. With several top-ranked hits consisting of immune pathways related to cytokine signaling (IL-4, IL-13, IL-10, and transforming growth factor β [TGF-β] signaling) and signal transduction and transcription (an NGF-TRKA signaling axis, nuclear events, and RAF-independent mitogen-activated protein kinase (MAPK) 1/3 activation) and an estrogen-dependent pathway (Figure 3F), our results inferred a possible sex-specific immune response of these CD161^{hi} cells in COVID-19.

Considering the critical roles of MOs in activating MAIT cells[33] and the association of dysregulated MOs with severe COVID-19 outcomes,[12,13,20,34] we applied the CellphoneDB package[35] and analyzed ligand-receptor interactions between MO and T cell clusters in our data. We identified 5 MO clusters, including three conventional subsets (classical, non-classical, and intermediate) and two subsets of activated MOs (CD16 MO$_A$ and CD14 MO$_A$) associated with COVID-19 (Figures 4A and 4B). These two activated MO subsets, which were also reported by other studies,[13,34] express high levels of interferon-related genes (Figure S3B). Although cell-cell communications may not take place in the blood in the same way as in solid tissue, our results inferred unique interactions between CD161^{hi} cells and MOs with the following gene pairs: *KLRB1_CLEC2D*, *CCL5_CCR1*, *CXCR6_CXCL16*, and *IL18_IL-18R* (Figures 4C and 4D). Moreover, the number of interaction counts of MOs was most abundant with the CD161^{hi} cluster relative to all major T cell populations (Figure 4E). A recent study reported IL-18-dependent MAIT cell activation by SARS-CoV-2-infected macrophages, which supports the existence of unique interactions of MAIT cells with MOs/macrophages in COVID-19.[27] These transcriptome findings further suggest a role of circulating CD161^{hi} cells in the SARS-CoV-2 immune response and their possible interactions with MO-derived cells.

Sex-specific heterogeneity of circulating MAIT cells in COVID-19

To analyze our scRNA-seq dataset for potential sex differences in circulating CD161^{hi} cells, we first sought to examine phenotypic heterogeneity in this population. To do this, we performed a focused subcluster analysis, which generated 3 distinct clusters (Figure 5A). However, this added resolution revealed a cluster that expressed *TRDC*, encoding the constant region of the δ chain expressed by γδ T cells (Figure 5B), which was excluded from subsequent analyses. In contrast, the other two clusters had higher *KLRB1* and *TRAV1-2* expression (Figure 5B), and they are therefore referred to here as MAITα and MAITβ clusters. Of note, these 2 clusters make up approximately 80% of CD161^{hi} PBMCs, which is consistent with a previously reported frequencies of circulating MAIT cells.[24] Our results showed that the MAITα cluster possessed upregulated genes associated with cytotoxic T cells (*GNLY*, *CD8A*, and *CD8B*), migration/adhesion (*CXCR4* and *ITGB2*), and cytokine signaling (*IRF1*, *B2M*, *NFKBIA*, *JUNB*, and *FOS*) (Figure 5C; Table S3). Although the MAITα cluster showed expression of the hemoglobin B gene (*HBB*), this cluster did not express other hemoglobin genes (Figures S4A and S4B), and its HBB expression level was much lower than in red blood cells (RBCs), suggesting that this cluster is not contaminated with RBCs. The MAITβ cluster was enriched for genes of ribosomal proteins, apoptosis (*BAX* and *STUB1*), and the linker histone H1 associated with apoptosis (*HIST1H1C*, *HIST1H1D*, and *HIST1H1E*) (Figure 5C; Table S3). Gene enrichment analysis further supported a functional dichotomy for α and β clusters. Although MAITα was enriched with several immune process pathways (e.g., interferon γ [IFN-γ], IL-4, and IL-13 signaling as well as antigen processing and
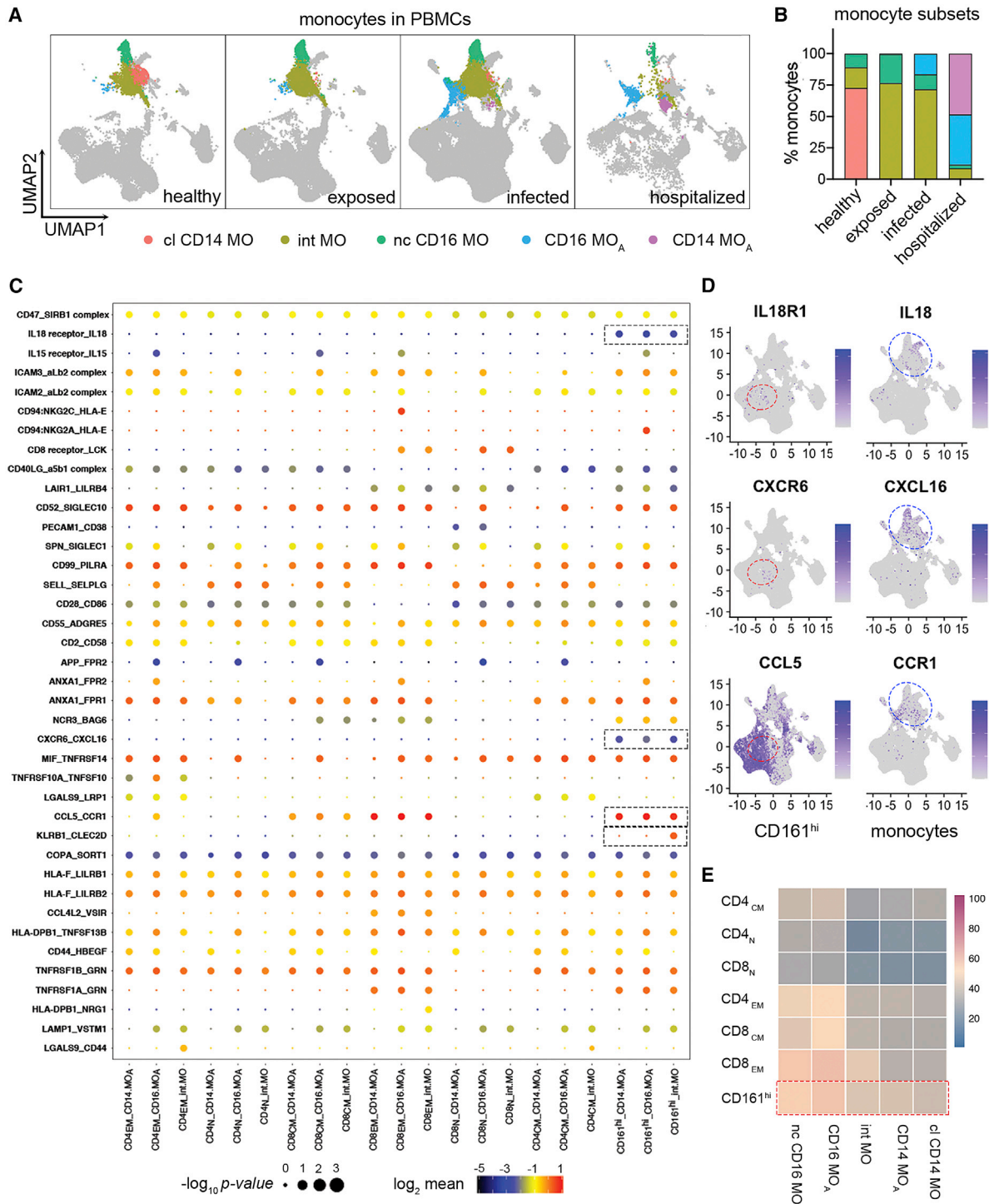
Figure 4. Receptor-ligand interaction inferences uncover unique interactions between CD8⁺CD161ʰⁱ T cells and MOs

(A and B) Visualization (A) and percentage distribution (B) of different MO subsets identified in Figure S3A. Three MO subsets represent resting classical (cl) CD14, non-classical (nc) CD16, and intermediate (int) MO as seen in healthy subjects. Two MO subsets involved in IFN signaling are associated with individuals with COVID-19. Based on differential expression of CD14 and CD16, they are referred to as activated CD14 and activated CD16 MO (CD14 MO$_A$ and CD16 MO$_A$, respectively).

(C) Overview of selected ligand-receptor interactions inferenced using CellPhoneDB in the COVID-19 PBMC single-cell dataset. The red box delineates specific interactions of CD161ʰⁱ T cells with MOs. p values and scales are indicated by circle size and color, respectively.

presentation), MAITβ was enriched in cellular responses to external stimuli, metabolism of RNA, viral infection, and programmed cell death but not immune processes (Figures 5D and 5E; Table S4). Hence our results suggest MAIT cell heterogeneity, with the MAITα signature representing an immunologically poised/active phenotype and the MAITβ signature representing a stressed/apoptotic phenotype.

Last for this series of experiments, we sought to determine the dynamics of the two phenotypically distinct clusters by sex over the COVID-19 disease course. By first grouping our data by severity and time after symptom onset, we found that MAITα was the major phenotype in healthy individuals, whereas MAITβ predominated in exposed and infected groups (Figures 5F and 5G) and at early, middle, and late time points (Figure 5H). There was a noted exception for hospitalized individuals (Figure 5F), who had very few cells, as seen in our flow cytometry data, consistent with lymphopenia, which occurs in severe COVID-19.[36] When further stratified by sex, we found that MAIT cell frequencies were higher in healthy females (Figures 5I and 5J), corroborating our flow cytometry results. In healthy females, these cells were skewed toward the MAITα cluster, whereas the few cells present in healthy males consisted mostly of the MAITβ cluster (Figure 5I). However, this difference was lost in the exposed/infected setting, where the cells of individuals of both sexes were comprised mostly of the MAITβ cluster (Figure 5J). Nonetheless, MAITβ cluster percentages were statistically greater in females in late disease (Figure 5J), which reflects the increased MAIT cells during late infection in females, as shown by our flow cytometry findings. Regarding expression of *CD69*, a T cell activation marker, we did not observe major differences across cluster or sex but did observe elevated expression in the hospitalized group (Figures S4C–S4F). This possibly suggests an altered MAIT cell response in hospitalized individuals.[24–27] These results suggest sex-specific MAIT cell differences at the quantitative and phenotypic levels in health and COVID-19.

Respiratory tract MAIT cell responses differ by sex in COVID-19

To test our hypothesis that the sex-specific change of circulating MAIT cells is due to their extravasation into airway tissues, we utilized published scRNA-seq datasets of bronchoalveolar lavage fluid (BALF)[37] and nasopharyngeal swabs (NPSs)[38] to assess MAIT cells in airway tissues of individuals with COVID-19. Beginning our analysis with the BALF dataset, we identified the MAIT cell cluster by expression of *TRAV1-2*, *CD3D*, *KLRB1*, and *SLC4A10* (Figures 6A–6C). With this annotation, we found a significant increase (p = 0.0188) of MAIT cells in individuals with COVID-19 (including mild and severe cases) relative to normal control individuals and a higher MAIT cell frequency (p = 0.0332) in females relative to males among subjects with COVID-19 (Figure 6D). This detection of increased MAIT cells in BALF from females, along with the drop in these cells we observed in peripheral blood from females, suggest female-dominant extravasation of MAIT cells in COVID-19.

To perform the same analysis with NPS samples, we integrated the T cell data from NPSs with those from BALF to identify MAIT cells in NPSs (Figure 6E and 6F) because TCR genes were not aligned in the NPS dataset.[38] With this annotation, we identified 232 and 631 MAIT cells in BALF and NPS, respectively, and quantified MAIT cell frequencies in the NPS dataset, again observing a significant increase (p = 0.0139) in individuals with COVID-19 (Figure 6G). We also analyzed the data across severity,

(D) Expression of representative ligand and receptor pairs between MAIT cells and MOs as indicated. Red and blue circles indicate CD161^hi clusters and MOs, respectively.
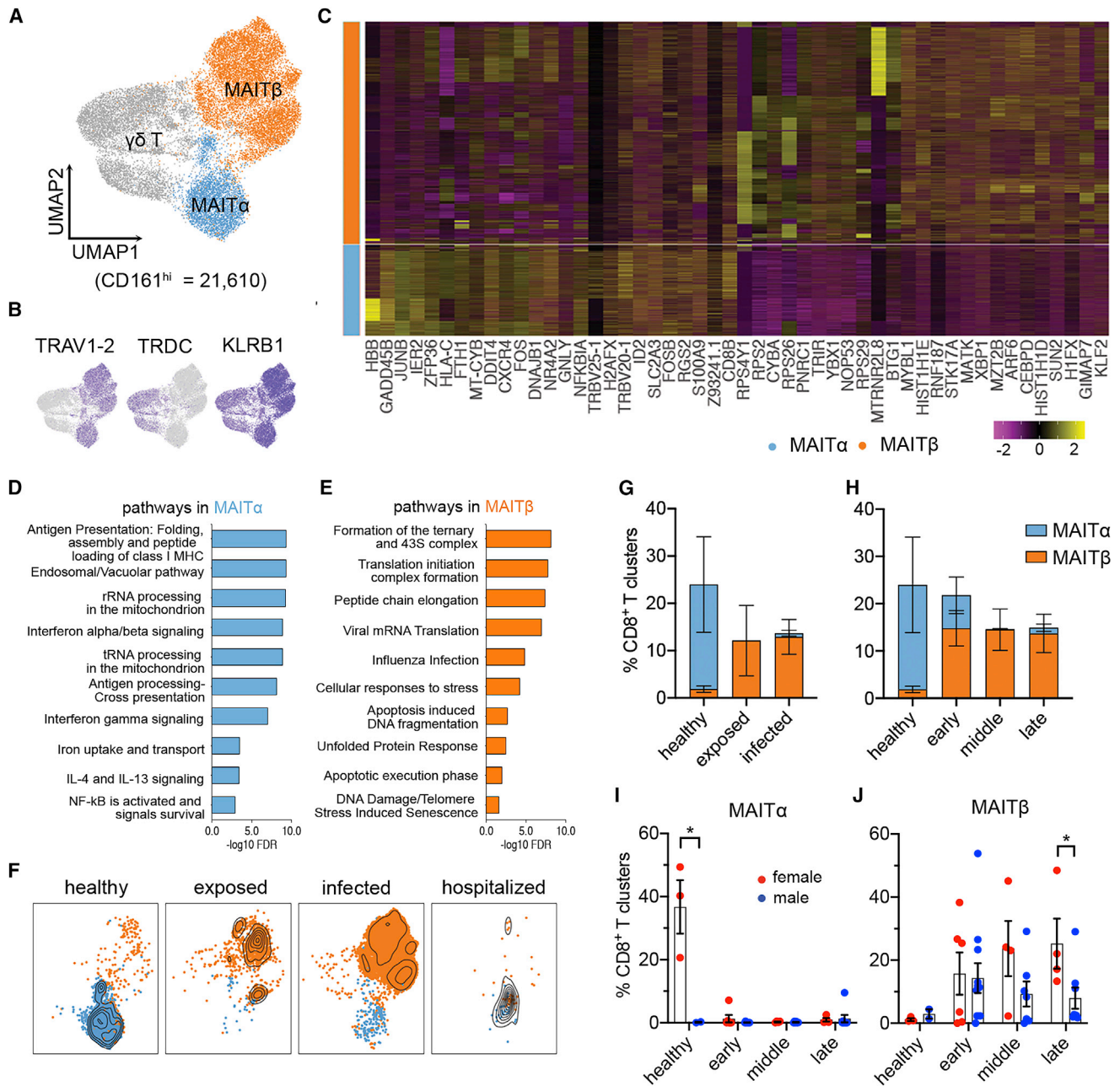(E) Heatmap of interaction counts between major T cell and MO subsets.

Figure 5. Heterogeneity and distinct dynamics of circulating MAIT cells across sexes in COVID-19

(A) Subclustering of CD161^{hi} cells (n = 21,610), showing two MAIT cell clusters and one γδ T cluster.

(B) Marker gene expression of three CD161^{hi} clusters.

(C) Heatmap of the top 25 discriminative genes between MAITα and MAITβ clusters. Expression level was scaled by Z score distribution.

(D and E) Representative top enriched pathways of MAITα and MAITβ in the Reactome Pathway Database (ranked by FDR, −log10 scale). The top 100 DEGs ranked by fold change between MAITα and MAITβ were used for this analysis.

(F and G) UMAP visualization of MAIT cluster changes (F) and their frequencies (G) with severity rank.

(H) Frequencies of MAIT clusters, grouped by time after symptom onset.

(I and J) Sex differences of MAIT clusters as shown in (H).

Data were plotted as mean ± standard error (G–J). Significance was determined by Mann-Whitney test (I). *p < 0.05. See also Figure S4 and Tables S3 and S4.

observing a significant increase (p = 0.0038) in subjects with moderate disease relative to normal subjects and a decrease (p = 0.0366) relative to individuals with critical COVID-19 (Figures 6H and 6I). We could not perform the same analysis by sex
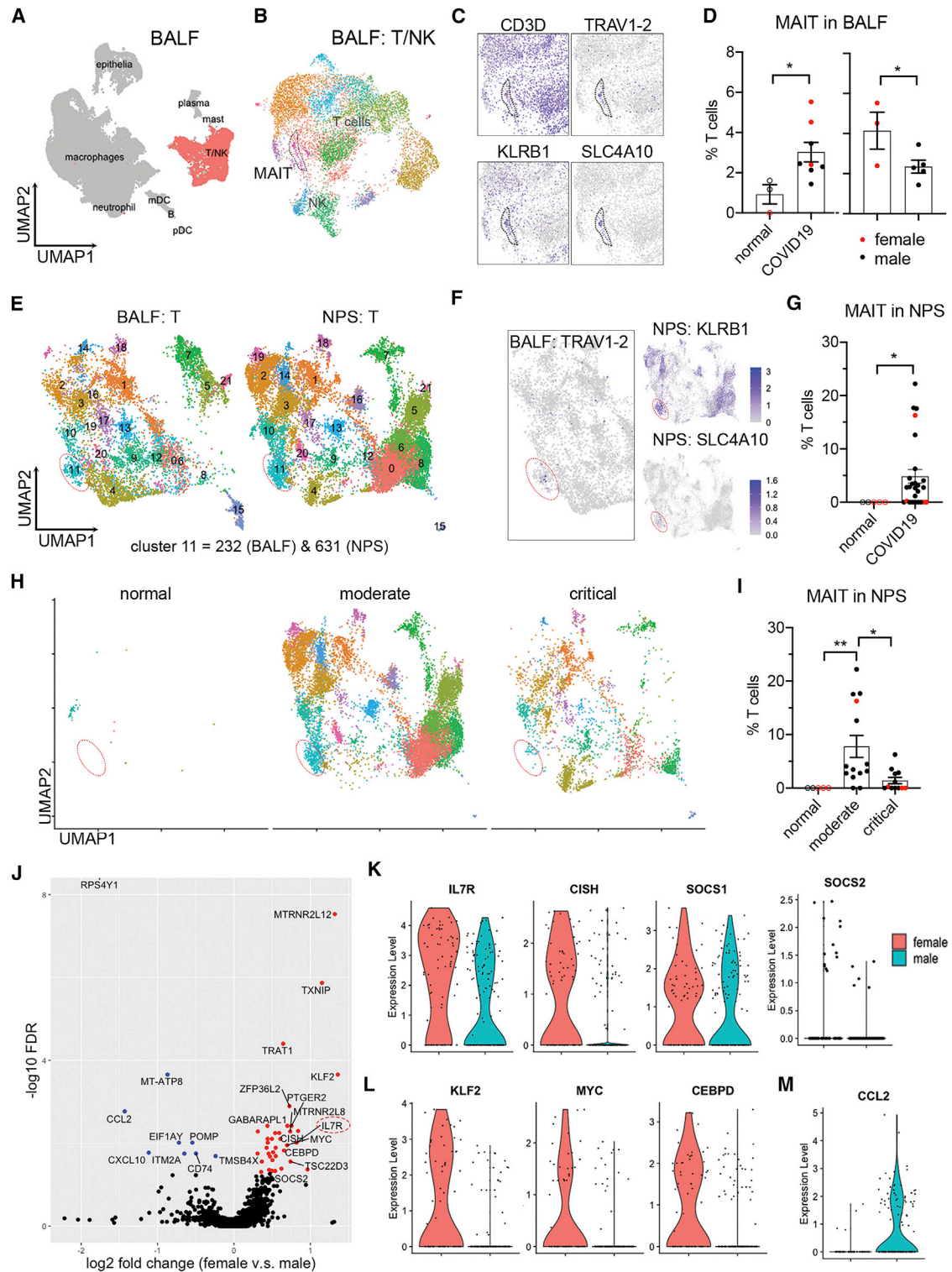
Figure 6. Sex differences of MAIT cells in airway tissue samples from individuals with COVID-19

(A and B) Clustering analysis of scRNA-seq data from the COVID-19 BALF dataset with subtracted T and NK cells.[37]

(C) MAIT cell cluster indicated by marker genes.

(D) Frequencies of MAIT cells in BALF between normal subjects and individuals with COVID-19 (left) and across sexes within subjects with COVID-19 (right).

because of insufficient numbers of samples from females (Figure 6I). Nonetheless, these results match the reduced circulating MAIT cell frequencies seen in our hospitalized individuals, suggesting that a lymphopenic state that occurs in severe COVID-19 affects MAIT cells, consistent with other reports.[24–26,39]

In a final experiment, we sought to characterize MAIT cell transcriptomes by sex in the BALF and NPS datasets and determine whether these cells resembled α and β phenotypes we identified in circulating MAIT cells. Cluster analysis was not warranted here, given the low cell numbers in these datasets. Instead, we leveraged gene modules derived from our respective α and β clusters of circulating MAIT cells. We found that MAIT cells in BALF and NPS data were largely skewed toward the β module, with minimal sex differences (Figure S5A). However, when we directly examined DEGs (DEGs between sexes), we were able to detect sex differences associated with α and β phenotypes. Specifically, in BALF, we found increased *IL7R* expression in females (Figure 6J) and other IL-7 signaling-associated genes (*CISH* and *SOCS1*) (Figure 6K). Given the key role of this signaling in T cell survival, we explored additional pathway genes, finding that female MAIT cells had upregulated anti-apoptotic genes (*BCL2* and *FOXP1*) and downregulated pro-apoptotic genes (*BAX* and *CASP3*) (Figures S5B and S5C). Also observed in cells from females were upregulated anti-proliferative genes (*CDKN1B* and *BTG2*) (Figure S5D). These patterns matched MAITα gene changes in our PBMC dataset. We were able to find other sex differences, including increased expression of several transcription factors (*KLF2*, *MYC*, and *CEBPD*) (Figure 6L). Conversely, males had higher expression of *CCL2* (Figure 6M), which has been linked to COVID-19 immunopathology.[40] In short, our results infer sex differences at the qualitative level in COVID-19, with MAIT cells from females possessing a pro-survival and immunologically active phenotype.

DISCUSSION

Despite the knowledge of sex differences in the immune response as an underlying factor in COVID-19 disease outcomes, the sexually dimorphic responses of MAIT cells, an unconventional T cell population deemed important in this disease, has remained unknown. Although MAIT cells may be known primarily for their role in host defense against bacteria, responding via their invariant TCRs to microbial vitamin B metabolites presented on major histocompatibility complex class I-related molecules,[33,41] they are also capable of responding in a TCR-independent manner to cytokines such as IL-12 and IL-18 and can be critical players in immune responses against certain viruses.[42–44] We now demonstrate that MAIT cells in females are quantitatively and qualitatively more robust in the SARS-CoV-2 setting, potentially helping us understand the immunological reasons for reduced COVID-19 susceptibility of females.

Our finding that MAIT cell recruitment to airway tissues may be more robust in females with COVID-19 was aided first by our observation of higher frequencies of circulating MAIT cells in females in the healthy setting. This difference can be explained by the

(E) Integrated clustering analysis of NPSs with BALF using Seurat 3. Cluster 11, MAIT cells.

(F) Referenced MAIT cell cluster in NPSs by expression of TRAV1-2 in BALF and the indicated marker genes in NPSs.

(G) Frequencies of MAIT cells in NPSs from healthy subjects and subjects with COVID-19.

(H and I) Visualization (H) and frequencies (I) of MAIT cells in NPSs, grouped by disease severity.

(J) Volcano plot showing DEGs of BALF MAIT cells between sex with log2 fold change and −log10 FDR.

(K–M) Expression of DEGs in IL-7 signaling (K), transcription factors (L), and CCL2 (M).

Data were plotted as mean ± standard error (D, G, and I), with females in red and males in black. Significance was determined by unpaired one-tailed Student's t test (D), Mann-Whitney test (G), and Kruskal-Wallis test with Dunn's post hoc test (I): *p < 0.05, **p < 0.01. See also Figure S5.

rate of physiological aging-related attrition of MAIT cells, which is substantially less pronounced in the blood of females.[45–47] The resultant higher frequencies in circulation enabled us to readily uncover the precipitous percentage drop we saw with MAIT cells relative to exposed/infected females. When trying to elucidate the potential cause of this drop, we considered two possible scenarios, (1) lymphopenia and (2) extravasation, which are not necessarily mutually exclusive. It is accepted that lymphopenia is associated with severe COVID-19 infection,[32,36,48,49] which agrees with our observations in our hospitalized group (comprised of 77.8% of individuals in intensive care). Similarly, lymphopenia could partially explain the reduction in MAIT cells described by Jouan et al.,[26] who studied male-dominated samples from critically ill individuals with COVID-19, although extravasation also likely occurred. In our study, however, we demonstrated that the frequencies of circulating MAIT cells dropped in our group of infected individuals. Because these subjects were not critically ill, our findings point to extravasation as a major reason for the sex-specific drop in the frequencies of circulating MAIT cells. The same pattern may also exist in several other studies.[24,25,27] For example, although it has been demonstrated that circulating MAIT cells are reduced in individuals with moderate COVID-19 relative to healthy subjects in aggregated data,[24] it is possible that the frequencies in healthy females contributed to reaching a statistical difference. Further supporting our conclusion, we were able to show, with publicly available scRNA-seq data from COVID-19 BALF samples,[37] that females in that study had an increased MAIT cell percentage relative to males, allowing us to conclude that MAIT cell extravasation during COVID-19 may be quantitatively more robust in females.

Our results also suggest that MAIT cells may be qualitatively superior in females with respect to anti-viral immune activity in COVID-19. Leading us to this conclusion, our scRNA-seq analysis of PBMCs from affected individuals revealed two distinct clusters of MAIT cells, MAITα and MAITβ. The α cluster was enriched for various immune pathways, such as IFN-γ signaling, inferring a capacity for anti-viral immune function. In contrast, the β cluster was enriched for cell stress and apoptosis pathways, inferring a frail phenotype roughly similar to a previously described population of double-negative MAIT cells.[50,51] We showed in the healthy setting that MAIT cells in females were skewed toward the α cluster, whereas those in males were comprised of the β cluster. Although, from these results, it could be inferred that the α cluster should be overrepresented in airways of females with COVID-19, this was not the case with BALF. However, we reasoned that such a finding would be very difficult to prove for two main reasons. First, extravasated MAIT cells with an α phenotype would be restricted to the early wave of recruitment because circulating cells are almost completely skewed to the β module in exposed/infected individuals. Second, a certain level of transcriptional reprogramming would occur upon immune cell extravasation into the tissue and potentially again upon accessing the alveolar space. Still, we were able to show in BALF that certain gene patterns remained consistent with the α signature in females versus males. In addition, our finding that BALF samples from females had quantitatively more MAIT cells gives further credence that differences revealed in the blood would likewise extend to tissue.

Limitations of study

The following limitations of this study should be considered when interpreting results. It is possible that decreased COVID-19 severity and elevated levels of MAIT cells are associated independently with the female sex. We showed the immunologically active signature of MAIT cells from females at the transcriptomic level, but functional analysis of MAIT cells in SARS-CoV-2 infection would be needed to demonstrate whether MAIT cells directly protect females with COVID-19. The same argument is relevant with respect to MAITα and MAITβ subsets in lung

tissues of individuals with COVID-19. Last, although our analyses included over 80 sex-balanced samples, the current study may not be powered to distinguish other immune cell types or specific sequelae that are associated with sex differences in COVID-19, and larger cohorts with more comprehensive longitudinal sampling would be needed in the future.

We conclude that MAIT cells in females are quantitatively and qualitatively distinct from those of males, and we surmise that this distinction provides a protective advantage in COVID-19. Indeed, females in general tend to have elevated frequencies of circulating MAIT cells, as also gleaned from large independent studies with European[45], South Korean,[46] and Chinese populations.[47] Further supporting this argument, it has now been recorded that fatality rates of adults with COVID-19 tend to be lower in females at all ages in 37 of 38 different countries or regions where MAIT cell frequencies tend to be higher in females, including North America, Europe, and Asia.[2] These points also argue against the possibility that an immunologically more robust MAIT cell response has a net negative effect; for example, by immunological misfiring[20] or cytokine storm-related immunopathology.[40] However, one open question our findings raise is whether the males in our study, who had more circulating CD8$^+$ memory T cells, would have an advantage in the reinfection setting or following vaccination.[52] Future studies are needed to explore this question and to better understand sex differences in MAIT cells in general and in COVID-19.

STAR★METHODS

Detailed methods are provided in the online version of this paper and include the following:

- KEY RESOURCES TABLE
- RESOURCE AVAILABILITY
  - Lead contact
  - Materials availability
  - Data and code availability
- EXPERIMENTAL MODEL AND SUBJECT DETAILS
  - Ethics statement
  - Participants in this study
- METHOD DETAILS
  - Collection of peripheral blood mononuclear cells (PBMCs)
  - Sample processing for flow cytometry and single cell RNA-sequencing (scRNA-seq)
  - Panel and Staining for Flow Cytometry
  - 36-color Full Spectrum Flow Cytometry
  - High-dimensional data analysis of flow cytometry data
  - ScRNA-seq using 10x Genomics platform
  - Processing and quality control of scRNA-seq
- QUANTIFICATION AND STATISTICAL ANALYSIS
  - Dimensionality reduction and clustering analysis
  - Differential gene expression analysis
  - Pathway enrichment analysis
  - Inference of ligand-receptor interactions between T cells and monocytes
  - Integration of BALF and NPS dataset
  - Calculations of the feature scores in MAIT cells
  - Statistical analysis

SUPPLEMENTAL INFORMATION

Supplemental information can be found online at https://doi.org/10.1016/j.medj.2021.04.008.

ACKNOWLEDGMENTS

AUTHOR CONTRIBUTIONS

C.Y., S.L., X.S., and D.R.S. designed the experiments. C.Y., S.L., M.T.M., C.W.W., X.S., and D.R.S. helped conceive and implement the study. C.Y., S.L., and D.R.S. performed data analyses, interpreted the data, and wrote the manuscript, which was critically revised by all other authors. E.R.K., E.L.T., M.T.M., and C.W.W. contributed to clinical study design. M.T.M., E.P., and T.W.B. acquired clinical samples and patient metadata. C.Y., R.M., and J.K. performed flow cytometry. N.S.G., S.D., H.A.C., G.O.R., T.R., and R.X. performed sample preparation and single-cell sequencing. G.D.S. and T.N.D. performed serology and PCR assessments.

DECLARATION OF INTERESTS

REFERENCES

1. Dong, E., Du, H., and Gardner, L. (2020). An interactive web-based dashboard to track COVID-19 in real time. Lancet Infect. Dis. *20*, 533–534.

2. Scully, E.P., Haverfield, J., Ursin, R.L., Tannenbaum, C., and Klein, S.L. (2020). Considering how biological sex impacts immune responses and COVID-19 outcomes. Nat. Rev. Immunol. *20*, 442–447.

3. Alghamdi, I.G., Hussain, I.I., Almalki, S.S., Alghamdi, M.S., Alghamdi, M.M., and El-Sheemy, M.A. (2014). The pattern of Middle East respiratory syndrome coronavirus in Saudi Arabia: a descriptive epidemiological analysis of data from the Saudi Ministry of Health. Int. J. Gen. Med. *7*, 417–423.

4. Karlberg, J., Chong, D.S., and Lai, W.Y. (2004). Do men have a higher case fatality rate of severe acute respiratory syndrome than women do? Am. J. Epidemiol. *159*, 229–231.

5. Leong, H.N., Earnest, A., Lim, H.H., Chin, C.F., Tan, C., Puhaindran, M.E., Tan, A., Chen, M.I., and Leo, Y.S. (2006). SARS in Singapore–predictors of disease severity. Ann. Acad. Med. Singap. 35, 326–331.

6. Channappanavar, R., Fett, C., Mack, M., Ten Eyck, P.P., Meyerholz, D.K., and Perlman, S. (2017). Sex-Based Differences in Susceptibility to Severe Acute Respiratory Syndrome Coronavirus Infection. J. Immunol. 198, 4046–4053.

7. Klein, S.L., and Flanagan, K.L. (2016). Sex differences in immune responses. Nat. Rev. Immunol. 16, 626–638.

8. Polanczyk, M.J., Carson, B.D., Subramanian, S., Afentoulis, M., Vandenbark, A.A., Ziegler, S.F., and Offner, H. (2004). Cutting edge: estrogen drives expansion of the CD4+CD25+ regulatory T cell compartment. J. Immunol. 173, 2227–2230.

9. Furman, D., Hejblum, B.P., Simon, N., Jojic, V., Dekker, C.L., Thiébaut, R., Tibshirani, R.J., and Davis, M.M. (2014). Systems analysis of sex differences reveals an immunosuppressive role for testosterone in the response to influenza vaccination. Proc. Natl. Acad. Sci. USA 111, 869–874.

10. Griesbeck, M., Ziegler, S., Laffont, S., Smith, N., Chauveau, L., Tomezsko, P., Sharei, A., Kourjian, G., Porichis, F., Hart, M., et al. (2015). Sex Differences in Plasmacytoid Dendritic Cell Levels of IRF5 Drive Higher IFN-α Production in Women. J. Immunol. 195, 5327–5336.

11. Mathew, D., Giles, J.R., Baxter, A.E., Oldridge, D.A., Greenplate, A.R., Wu, J.E., Alanio, C., Kuri-Cervantes, L., Pampena, M.B., D'Andrea, K., et al.; UPenn COVID Processing Unit (2020). Deep immune profiling of COVID-19 patients reveals distinct immunotypes with therapeutic implications. Science 369, eabc8511.

12. Silvin, A., Chapuis, N., Dunsmore, G., Goubet, A.G., Dubuisson, A., Derosa, L., Almire, C., Hénon, C., Kosmider, O., Droin, N., et al. (2020). Elevated Calprotectin and Abnormal Myeloid Cell Subsets Discriminate Severe from Mild COVID-19. Cell 182, 1401–1418.e18.

13. Schulte-Schrepping, J., Reusch, N., Paclik, D., Baßler, K., Schlickeiser, S., Zhang, B., Krämer, B., Krammer, T., Brumhard, S., Bonaguro, L., et al.; Deutsche COVID-19 OMICS Initiative (DeCOI) (2020). Severe COVID-19 Is Marked by a Dysregulated Myeloid Cell Compartment. Cell 182, 1419–1440.e23.

14. Mann, E.R., Menon, M., Knight, S.B., Konkel, J.E., Jagger, C., Shaw, T.N., Krishnan, S., Rattray, M., Ustianowski, A., Bakerly, N.D., et al.; NIHR Respiratory TRC; CIRCO (2020). Longitudinal immune profiling reveals key myeloid signatures associated with COVID-19. Sci. Immunol. 5, eabd6197.

15. Peng, Y., Mentzer, A.J., Liu, G., Yao, X., Yin, Z., Dong, D., Dejnirattisai, W., Rostron, T., Supasa, P., Liu, C., et al.; Oxford Immunology Network Covid-19 Response T cell Consortium; ISARIC4C Investigators (2020). Broad and strong memory CD4+ and CD8+ T cells induced by SARS-CoV-2 in UK convalescent individuals following COVID-19. Nat. Immunol. 21, 1336–1345.

16. Sekine, T., Perez-Potti, A., Rivera-Ballesteros, O., Strålin, K., Gorin, J.B., Olsson, A., Llewellyn-Lacey, S., Kamal, H., Bogdanovic, G., Muschiol, S., et al.; Karolinska COVID-19 Study Group (2020). Robust T Cell Immunity in Convalescent Individuals with Asymptomatic or Mild COVID-19. Cell 183, 158–168.e14.

17. Le Bert, N., Tan, A.T., Kunasegaran, K., Tham, C.Y.L., Hafezi, M., Chia, A., Chng, M.H.Y., Lin, M., Tan, N., Linster, M., et al. (2020). SARS-CoV-2-specific T cell immunity in cases of COVID-19 and SARS, and uninfected controls. Nature 584, 457–462.

18. Weiskopf, D., Schmitz, K.S., Raadsen, M.P., Grifoni, A., Okba, N.M.A., Endeman, H., van den Akker, J.P.C., Molenkamp, R., Koopmans, M.P.G., van Gorp, E.C.M., et al. (2020). Phenotype and kinetics of SARS-CoV-2-specific T cells in COVID-19 patients with acute respiratory distress syndrome. Sci. Immunol. 5, eabd2071.

19. Del Valle, D.M., Kim-Schulze, S., Huang, H.H., Beckmann, N.D., Nirenberg, S., Wang, B., Lavin, Y., Swartz, T.H., Madduri, D., Stock, A., et al. (2020). An inflammatory cytokine signature predicts COVID-19 severity and survival. Nat. Med. 26, 1636–1643.

20. Takahashi, T., Ellingson, M.K., Wong, P., Israelow, B., Lucas, C., Klein, J., Silva, J., Mao, T., Oh, J.E., Tokuyama, M., et al.; Yale IMPACT Research Team (2020). Sex differences in immune responses that underlie COVID-19 disease outcomes. Nature 588, 315–320.

21. McClain, M.T., Constantine, F.J., Henao, R., Liu, Y., Tsalik, E.L., Burke, T.W., Steinbrink, J.M., Petzold, E., Nicholson, B.P., Rolfe, R., et al. (2020). Dysregulated transcriptional responses to SARS-CoV-2 in the periphery support novel diagnostic approaches. medRxiv. https://doi.org/10.1101/2020.07.20.20155507.

22. Becht, E., McInnes, L., Healy, J., Dutertre, C.A., Kwok, I.W.H., Ng, L.G., Ginhoux, F., and Newell, E.W. (2018). Dimensionality reduction for visualizing single-cell data using UMAP. Nat. Biotechnol. Published online December 3, 2018. https://doi.org/10.1038/nbt.4314.

23. Van Gassen, S., Callebaut, B., Van Helden, M.J., Lambrecht, B.N., Demeester, P., Dhaene, T., and Saeys, Y. (2015). FlowSOM: Using self-organizing maps for visualization and interpretation of cytometry data. Cytometry A 87, 636–645.

24. Parrot, T., Gorin, J.B., Ponzetta, A., Maleki, K.T., Kammann, T., Emgård, J., Perez-Potti, A., Sekine, T., Rivera-Ballesteros, O., Gredmark-Russ, S., et al.; Karolinska COVID-19 Study Group (2020). MAIT cell activation and dynamics associated with COVID-19 disease severity. Sci. Immunol. 5, eabe1670.

25. Kuri-Cervantes, L., Pampena, M.B., Meng, W., Rosenfeld, A.M., Ittner, C.A.G., Weisman, A.R., Agyekum, R.S., Mathew, D., Baxter, A.E., Vella, L.A., et al. (2020). Comprehensive mapping of immune perturbations associated with severe COVID-19. Sci. Immunol. 5, eabd7114.

26. Jouan, Y., Guillon, A., Gonzalez, L., Perez, Y., Boisseau, C., Ehrmann, S., Ferreira, M., Daix, T., Jeannet, R., François, B., et al. (2020). Phenotypical and functional alteration of unconventional T cells in severe COVID-19 patients. J. Exp. Med. 217, e20200872.

27. Flament, H., Rouland, M., Beaudoin, L., Toubal, A., Bertrand, L., Lebourgeois, S., Rousseau, C., Soulard, P., Gouda, Z., Cagninacci, L., et al. (2021). Outcome of SARS-CoV-2 infection is linked to MAIT cell activation and cytotoxicity. Nat. Immunol. 22, 322–335.

28. Stuart, T., Butler, A., Hoffman, P., Hafemeister, C., Papalexi, E., Mauck, W.M., 3rd, Hao, Y., Stoeckius, M., Smibert, P., and Satija, R. (2019). Comprehensive Integration of Single-Cell Data. Cell 177, 1888–1902.e21.

29. Chen, G., Wu, D., Guo, W., Cao, Y., Huang, D., Wang, H., Wang, T., Zhang, X., Chen, H., Yu, H., et al. (2020). Clinical and immunological features of severe and moderate coronavirus disease 2019. J. Clin. Invest. 130, 2620–2629.

30. Zhao, Q., Meng, M., Kumar, R., Wu, Y., Huang, J., Deng, Y., Weng, Z., and Yang, L. (2020). Lymphopenia is associated with severe coronavirus disease 2019 (COVID-19) infections: A systemic review and meta-analysis. Int. J. Infect. Dis. 96, 131–135.

31. Tan, L., Wang, Q., Zhang, D., Ding, J., Huang, Q., Tang, Y.Q., Wang, Q., and Miao, H. (2020). Lymphopenia predicts disease severity of COVID-19: a descriptive and predictive study. Signal Transduct. Target. Ther. 5, 33.

32. Huang, C., Wang, Y., Li, X., Ren, L., Zhao, J., Hu, Y., Zhang, L., Fan, G., Xu, J., Gu, X., et al. (2020). Clinical features of patients infected with 2019 novel coronavirus in Wuhan, China. Lancet 395, 497–506.

33. Godfrey, D.I., Koay, H.F., McCluskey, J., and Gherardin, N.A. (2019). The biology and functional importance of MAIT cells. Nat. Immunol. 20, 1110–1128.

34. Wilk, A.J., Rustagi, A., Zhao, N.Q., Roque, J., Martínez-Colón, G.J., McKechnie, J.L., Ivison, G.T., Ranganath, T., Vergara, R., Hollis, T., et al. (2020). A single-cell atlas of the peripheral immune response in patients with severe COVID-19. Nat. Med. 26, 1070–1076.

35. Efremova, M., Vento-Tormo, M., Teichmann, S.A., and Vento-Tormo, R. (2020). CellPhoneDB: inferring cell-cell communication from combined expression of multi-subunit ligand-receptor complexes. Nat. Protoc. 15, 1484–1506.

36. Chen, Z., and John Wherry, E. (2020). T cell responses in patients with COVID-19. Nat. Rev. Immunol. 20, 529–536.

37. Liao, M., Liu, Y., Yuan, J., Wen, Y., Xu, G., Zhao, J., Cheng, L., Li, J., Wang, X., Wang, F., et al. (2020). Single-cell landscape of bronchoalveolar immune cells in patients with COVID-19. Nat. Med. 26, 842–844.

38. Chua, R.L., Lukassen, S., Trump, S., Hennig, B.P., Wendisch, D., Pott, F., Debnath, O., Thürmann, L., Kurth, F., Völker, M.T., et al. (2020). COVID-19 severity correlates with airway epithelium-immune cell interactions identified by single-cell analysis. Nat. Biotechnol. 38, 970–979.

39. De Biasi, S., Meschiari, M., Gibellini, L., Bellinazzi, C., Borella, R., Fidanza, L., Gozzi, L., Iannone, A., Lo Tartaro, D., Mattioli, M., et al. (2020). Marked T cell activation, senescence, exhaustion and skewing towards TH17 in patients with COVID-19 pneumonia. Nat. Commun. 11, 3434.

40. Merad, M., and Martin, J.C. (2020). Pathological inflammation in patients with COVID-19: a key role for monocytes and macrophages. Nat. Rev. Immunol. *20*, 355–362.

41. Kjer-Nielsen, L., Patel, O., Corbett, A.J., Le Nours, J., Meehan, B., Liu, L., Bhati, M., Chen, Z., Kostenko, L., Reantragoon, R., et al. (2012). MR1 presents microbial vitamin B metabolites to MAIT cells. Nature *491*, 717–723.

42. van Wilgenburg, B., Scherwitzl, I., Hutchinson, E.C., Leng, T., Kurioka, A., Kulicke, C., de Lara, C., Cole, S., Vasanawathana, S., Limpitikul, W., et al.; STOP-HCV consortium (2016). MAIT cells are activated during human viral infections. Nat. Commun. *7*, 11653.

43. Ussher, J.E., Bilton, M., Attwod, E., Shadwell, J., Richardson, R., de Lara, C., Mettke, E., Kurioka, A., Hansen, T.H., Klenerman, P., and Willberg, C.B. (2014). CD161++ CD8+ T cells, including the MAIT cell subset, are specifically activated by IL-12+IL-18 in a TCR-independent manner. Eur. J. Immunol. *44*, 195–203.

44. van Wilgenburg, B., Loh, L., Chen, Z., Pediongco, T.J., Wang, H., Shi, M., Zhao, Z., Koutsakos, M., Nüssing, S., Sant, S., et al. (2018). MAIT cells contribute to protection against lethal influenza infection in vivo. Nat. Commun. *9*, 4706.

45. Novak, J., Dobrovolny, J., Novakova, L., and Kozak, T. (2014). The decrease in number and change in phenotype of mucosal-associated invariant T cells in the elderly and differences in men and women of reproductive age. Scand. J. Immunol. *80*, 271–275.

46. Lee, O.J., Cho, Y.N., Kee, S.J., Kim, M.J., Jin, H.M., Lee, S.J., Park, K.J., Kim, T.J., Lee, S.S., Kwon, Y.S., et al. (2014). Circulating mucosal-associated invariant T cell levels and their cytokine levels in healthy adults. Exp. Gerontol. *49*, 47–54.

47. Chen, P., Deng, W., Li, D., Zeng, T., Huang, L., Wang, Q., Wang, J., Zhang, W., Yu, X., Duan, D., et al. (2019). Circulating Mucosal-Associated Invariant T Cells in a Large Cohort of Healthy Chinese Individuals From Newborn to Elderly. Front. Immunol. *10*, 260.

48. Chen, N., Zhou, M., Dong, X., Qu, J., Gong, F., Han, Y., Qiu, Y., Wang, J., Liu, Y., Wei, Y., et al. (2020). Epidemiological and clinical characteristics of 99 cases of 2019 novel coronavirus pneumonia in Wuhan, China: a descriptive study. Lancet *395*, 507–513.

49. Laing, A.G., Lorenc, A., Del Molino Del Barrio, I., Das, A., Fish, M., Monin, L., Muñoz-Ruiz, M., McKenzie, D.R., Hayday, T.S., Francos-Quijorna, I., et al. (2020). A dynamic COVID-19 immune signature includes associations with poor prognosis. Nat. Med. *26*, 1623–1635.

50. Gérart, S., Sibéril, S., Martin, E., Lenoir, C., Aguilar, C., Picard, C., Lantz, O., Fischer, A., and Latour, S. (2013). Human iNKT and MAIT cells exhibit a PLZF-dependent proapoptotic propensity that is counterbalanced by XIAP. Blood *121*, 614–623.

51. Dias, J., Leeansyah, E., and Sandberg, J.K. (2017). Multiple layers of heterogeneity and subset diversity in human MAIT cell responses to distinct microorganisms and to innate cytokines. Proc. Natl. Acad. Sci. USA *114*, E5434–E5443.

52. Provine, N.M., Amini, A., Garner, L.C., Spencer, A.J., Dold, C., Hutchings, C., Silva Reyes, L., FitzPatrick, M.E.B., Chinnakannan, S., Oguti, B., et al. (2021). MAIT cell activation augments adenovirus vector vaccine immunogenicity. Science *371*, 521–526.

53. Love, M.I., Huber, W., and Anders, S. (2014). Moderated estimation of fold change and dispersion for RNA-seq data with DESeq2. Genome Biol. *15*, 550.

54. Tirosh, I., Izar, B., Prakadan, S.M., Wadsworth, M.H., 2nd, Treacy, D., Trombetta, J.J., Rotem, A., Rodman, C., Lian, C., Murphy, G., et al. (2016). Dissecting the multicellular ecosystem of metastatic melanoma by single-cell RNA-seq. Science *352*, 189–196.

STAR★METHODS

KEY RESOURCES TABLE

REAGENT or RESOURCE	SOURCE	IDENTIFIER
Antibodies		
BV421 anti-human CCR7 (clone G043H7)	BioLegend	Cat# 353208
BV711 anti-human CCR6 (clone G034E3)	BioLegend	Cat# 353436
BV750 anti-huamn CXCR5 (clone RF8B2)	BD Biosicences	Cat# 747111
BUV563 anti-huamn CCR5 (clone 2D7)	BD Biosicences	Cat# 741401
PE-Cyanine7 anti-human CXCR3 (clone CEW33D)	ThermoFisher	Cat# 25-1839-42
PerCP-eFluor710 anti-human TCR γδ (clone B1.1)	ThermoFisher	Cat# 46-9959-42
APC-Fire810 anti-human CD38 (clone HIT2)	BioLegend	Cat# 303549
FITC anti-human CD57 (clone HNK-1)	BioLegend	Cat# 359604
PE-Cyanine5 anti-huamn CD95 (clone DX2)	ThermoFisher	Cat# 15-0959-42
Spark-NIR685 anti-huamn CD19 (clone H1B19)	BioLegend	Cat# 302270
Spark-NIR550 anti-human CD14 (clone 63D3)	BioLegend	Cat# 367148
PerCP anti-human CD45 (clone H130)	ThermoFisher	Cat# MHCD4531
PE anti-huamn CD25 (clone BC96)	ThermoFisher	Cat# 12-0259-42
APC anti-human CD27 (clone O323)	ThermoFisher	Cat# 17-0279-42
APC-eFluor780 anti-human HLA-DR (clone L243)	ThermoFisher	Cat# 47-9952-42
PerCP-Cyanine5.5 anti-human CD11b (clone ICRF44)	BioLegend	Cat# 301328
PE-eFluor610 anti-human CD24 (clone eBioSN3 (SN3 A5-2H10))	ThermoFisher	Cat# 61-0247-41
Alexa Fluor®647 anti-human CD1c (clone L161)	BioLegend	Cat# 331510
APC-R700 anti-human CD127 (clone HIL-7R-M21)	BD Biosicences	Cat# 565185
BUV496 anti-human CD16 (clone 3G8)	BD Biosicences	Cat# 612944
BV480 anti-human IgD (clone IA6-2)	BD Biosicences	Cat# 566138
BUV395 anti-human CD45RA (clone 5H9)	BD Biosicences	Cat# 740315
BUV737 anti-human CD56 (clone NCAM16.2)	BD Biosicences	Cat# 612766
BUV805 anti-human CD8 (clone SK1)	BD Biosicences	Cat# 612889
BUV661 anti-human CD11c (clone B-ly6)	BD Biosicences	Cat# 612967
SuperBright436 anti-human CD123 (clone 6H6)	ThermoFisher	Cat# 62-1239-42
BV570 anti-human IgM (clone MHM-88)	BioLegend	Cat# 314517
BV650 anti-human CD28 (clone CD28.2)	BioLegend	Cat# 302946
BB515 anti-human CD141 (clone 1A4)	BD Biosicences	Cat# 566017
eFluor450 anti-human CD161 (clone HP-3G10)	ThermoFisher	Cat# 48-1619-42
BV510 anti-human CD3 (clone OKT3)	BioLegend	Cat# 317332
Pacific Orange anti-human CD20 (clone HI47)	ThermoFisher	Cat# MHCD2030
BV605 anti-human IgG (clone G18-145)	BD Biosicences	Cat# 563246
BV785 anti-human PD-1 (clone EH12.2H7)	BioLegend	Cat# 329929
BUV615 anti-human CD4 (clone SK3)	BD Biosicences	Cat# 612987
Biological samples		
Peripheral blood from healthy and COVID-19 related subjects	Duke University Health System	NA
Chemicals, peptides, and recombinant rroteins		
Live/Dead UV Blue	ThermoFisher	Cat# L34962
Brilliant Stain Buffer Plus	BD Biosicences	Cat# 566385

(Continued on next page)

Continued

REAGENT or RESOURCE	SOURCE	IDENTIFIER
Critical commercial assays		
Dead Cell Removal Kit	Miltenyi Biotec	Cat# 130-090-101
Chromium Next GEM Single Cell 5′ Library & Gel Bead Kit v1	10x Genomics	
Deposited data		
BALF scRNA-seq data	Liao et al.[37]	GSE145926
NPS scRNA-seq data	Chua et al.[38]	https://figshare.com/articles/COVID-19_severity_correlates_with_airway_epithelium-immune_cell_interactions_identified_by_single-cell_analysis/12436517
Supplemental data	This study	https://dx.doi.org/10.17632/csc9p34d5t.1
scRNA-seq data of PBMCs	This study	GSE171555
Flow cytometry data of PBMCs	This study	https://flowrepository.org/id/FR-FCM-Z3WR
Software and algorithms		
FlowJo version 10.6.1	Tree Star	https://www.flowjo.com/
Omiq	Omiq	https://www.omiq.ai/
Cell Ranger version 3.1.0	10x Genomics	https://www.10xgenomics.com/
Seurat v3 R package		https://satijalab.org/seurat/
CellPhone DB v2		https://www.cellphonedb.org/
Reactome pathway database		https://reactome.org/
GraphPad Prism version 8		https://www.graphpad.com/

RESOURCE AVAILABILITY

Lead contact

Further information and requests for resources and reagents should be directed to and will be fulfilled by the Lead Contact, Daniel R. Saban (daniel.saban@duke.edu).

Materials availability

This study did not generate new unique reagents.

Data and code availability

Publicly available scRNA-seq data of BALF[37] were downloaded from GEO with the accession number GSE145926, and the count data of NPS[38] were downloaded from https://figshare.com/articles/COVID-19_severity_correlates_with_airway_epithelium-immune_cell_interactions_identified_by_single-cell_analysis/12436517. All clinical metadata of participants and samples in this study are included in Table S1. The fcs files of flow cytometry are available to download from https://flowrepository.org/id/FR-FCM-Z3WR. The scRNA-seq of PBMC data generated in this study are available in Gene Expression Omnibus (GEO) with the accession number GSE171555. Additional Supplemental Items are available from Mendeley Data at https://dx.doi.org/10.17632/csc9p34d5t.1. All analytic scripts will be also made available per request.

EXPERIMENTAL MODEL AND SUBJECT DETAILS

Ethics statement

This study and relevant protocols were approved by the Institutional Review Boards of Duke University Health System (DUHS). All procedures were performed in accordance with the Declaration of Helsinki, applicable regulations, and local policies.

Participants in this study

Inpatients (hospitalized) and outpatients (infected) with confirmed infection of SARS-CoV-2 were identified through the DUHS and enrolled into the Molecular and Epidemiological Study of Suspected Infection (MESSI, Pro00100241). The PCR testing for

SARS-CoV-2 was performed at either the North Carolina State Laboratory of Public Health or at clinical laboratories of the DUHS. The exposed group, who closely contacted with COVID-19 patients, presented negative PCR test and negative serology test during longitudinally sampling from the first visit to at least 2 months after, typically 0, 7, 14, and 28 days relative to enrollment. Initial severity scores of individuals were recorded through a self-reporting survey on 38 defined symptoms related to COVID-19 plus "other" when enrolled. The exposed group (average score = 9.71) showed a lower severity scores compared with infected (outpatients) group (average score = 18.16). The hospitalized patients presented severe disease symptoms with breath difficulty, cough, fever or chest pain when enrolled, and 77.8% of them for this study required intensive care unit (ICU) care. All COVID-19 patients were also longitudinally sampled with serology test from enrollment to convalescent phase. Healthy donors were enrolled in 2019 (Duke IRB Protocol Pro00009459) with no diagnosis or symptoms consistent with COVID-19 or other respiratory illness. Written informed consent was obtained from all subjects or legally authorized representatives. Patient Demographics are summarized in Tables 1 and S1.

In keeping with inclusion criteria above, all participants with the minimum age of 17 were maintained in the analysis. Investigators were blinded during experiments in terms of sex, time post symptom onset and anti-SARS-COV-2 IgG serology condition.

METHOD DETAILS

Collection of peripheral blood mononuclear cells (PBMCs)

Peripheral whole blood was collected in EDTA vacutainer tubes and processed within 8 hours via Ficoll-Hypaque density gradient method to obtain cryopreserved PBMCs. Blood was diluted 1:2 in PBS, layered onto the the Ficoll-Hypaque in 50 mL conicals, and centrifuged at 420 g for 25 min. Buffy coat was used to collect PBMCs and cell pellets were washed twice with D-PBS following centrifugation at 400 g for 10 min. Counts and cell viability were obtained using Vi-Cell automated cell counter (Beckman-Coulter) before PBMCs were adjusted to 10×10^6 cells/ml in cryopreservation media (90% FBS, 10% DMSO) and aliquoted into cryopreservation vials on ice. Finally, cells were subjected to controlled freezing at $-80°C$ using CoolCell LX (BioCision) for 12-24 hours, and transferred to liquid nitrogen vapor phase.

Sample processing for flow cytometry and single cell RNA-sequencing (scRNA-seq)

Counts and cell viability of thawed PBMCs were measured by Countess II after a wash with DMEM 10% FBS. The cell viability of hospitalized patients ranged from 70%–80% whereas all other samples exceeded 80% viability. An additional dead cell removal step (Miltenyi Biotec) was conducted on hospitalized PBMC samples prior to aliquot for scRNA-seq. To perform scRNA-seq, 200,000 cells per sample were aliquoted, spun down, resuspended in 30 μL PBS supplemented with 0.04% BSA and 0.2U/μl RNase inhibitor and counted using Countess II.

Panel and Staining for Flow Cytometry

Approximately 0.5-2×10^6 cells per cryopreserved sample were stained for flow cytometry analysis. Antibody titrations used in this study were previously established by Cytek Biosciences with slight modifications. All staining procedures were performed at room temperature. PBMCs were stained with live/dead Blue (Thermofisher) for 15 min, washed with FACS-EDTA buffer and spun down at 1500 rpm for 5 min. Samples were resuspended with Brilliant Stain Buffer Plus (BD Biosciences) and sequentially stained with anti-CCR7 for 10 min, all other chemokine receptor

mix of CCR6, CXCR5, CCR5 and CXCR3 for 5 min, anti-TCR gamma/delta for 10 min and the rest surface receptor mix for 30 min. After incubation, PBMCs were washed with FACS-EDTA buffer and spun down at 1500 rpm for 5 min. Samples were fixed with 1% PFA in PBS for 20 min, spun down and resuspended in FACS-EDTA buffer.

36-color Full Spectrum Flow Cytometry

Samples were acquired using a four-laser Cytek Aurora Spectral Flow Cytometry System. Single color controls for spectral unmixing were acquired with PBMCs from healthy control blood and UltraComp eBeads (ThermoFisher). Raw data were unmixed and further analyzed using either FlowJo for manual gating or Omiq (https://www.omiq.ai) for clustering visualization and analysis.

High-dimensional data analysis of flow cytometry data

Uniform Manifold Approximation and Projection (UMAP) and FlowSOM clustering analyses were performed on Omiq (https://www.omiq.ai), using equal random sampling of 3000 live CD45+ singlets. from each FCS file. The UMAP plot was generated with the parameters of 15 neighbors and 0.4 minimum distance. All markers in flow panel were used for analysis except live/dead and CD45.

ScRNA-seq using 10x Genomics platform

10x Genomics Single Cell 5′ v1 chemistry was used to generate Gel Bead-In Emulsions (GEM), and perform post GEM-RT cleanup, cDNA amplification, as well as library construction. An agilent DNA ScreenTape assay was used for quality control. Libraries were pooled and sequenced to saturation or 20,000 unique reads per cell on average using an Illumina NovaSeq6000 with 150-bp paired-end reads.

Processing and quality control of scRNA-seq

Raw sequencing data were initially processed with 10x Genomics Cell Ranger pipelines (V3.1.0). Briefly, BCL files were demultiplexed to generate FASTQ files. FASTQ files were aligned with STAR aligner to the human genome reference GRCh38 from Ensemble database. Feature barcode processing and UMI counting were then performed according to the standard workflow. (QC summary after sequencing). The following criteria were applied as quality control of single cells from all individual samples. Cells that had fewer than 1000 UMI counts or 500 genes, as well as cell that had greater than 10% of mitochondrial genes were removed from further analysis. Genes that were expressed by fewer than 10 cells were also excluded. After filtering, a total of 424,080 cells with 18,765 gene features were kept for the downstream analysis.

QUANTIFICATION AND STATISTICAL ANALYSIS

Dimensionality reduction and clustering analysis

The filtered gene-barcode matrix was analyzed using Seurat 3.[28] All the procedures were conducted with the default parameters unless otherwise specified. Briefly, data were first normalized using log transformation and adjusted with a scale factor of 10,000. The top 2,000 variable genes were identified, and percentages of mitochondrial genes were regressed out when scaling data. Principle component analysis (PCA) was performed using these top variable genes, and top 25 principle components (PCs) were selected for graph-based clustering with Shared Nearest Neighbor (SNN) and visualization in UMAP. The resolution was set to 0.35 to identify major immune cell subsets in PBMCs. Sub-clustering of CD161hi T cells (21,610 cells) was also performed using the analytic pipeline mentioned above with two modifications: top 10 PCs were used, and the resolution was set to 0.1 to identify MAIT cell clusters.

Differential gene expression analysis

Differentially expressed genes (DEGs) were identified using Seurat 3 (FindAllMarkers or FindMarkers Functions) with either 'wilcox' for all cluster markers or 'DESeq2'.[53] Randomly downsampled data with 100,000 cells were used to find all markers of PBMC clusters. A gene was considered significant with adjusted p value or false discovery rate (FDR) < 0.05. DEGs results of all PBMCs and MAIT cells are listed in Tables S2 and S3.

Pathway enrichment analysis

Top 100 DEGs of MAIT clusters were used for pathway enrichment analysis using Reactome Pathway Database (https://reactome.org). A pathway was considered significantly over-presented with FDR < 0.05. The full pathway enrichment results are summarized in Table S4.

Inference of ligand-receptor interactions between T cells and monocytes

Ligand-receptor interactions between T cells and monocytes were inferred using Cell-PhoneDB.[35] PBMC scRNA-seq data were randomly downsampled to 50,000 cells and T and monocyte clusters were extracted based on the expression of their lineage markers. CellPhoneDB was with default parameters (https://github.com/Teichlab/cellphonedb). The inferred interactions are considered significant when p value < 0.05.

Integration of BALF and NPS dataset

Publicly available scRNA-seq data of BALF[37] and of NPS[38] were downloaded and processed using Seurat 3 as previously described.[28] All T cell clusters, were extracted from both datasets and integrated via the Single Cell Transform (SCT) method in Seurat 3. Top 3,000 variable features were selected for the integration. Dimensionality reduction was conducted using PCA and UMAP embedding of the top 100 PCs. Clusters were visualized at a resolution of 0.8 after constructing a SNN graph using the first 50 PCs.

Calculations of the feature scores in MAIT cells

The DEGs between MAIT1 and MAIT2 were used to generate their feature scores as previously described.[54] The feature scores were calculated using AddModuleScore function in Seurat 3. MAIT cells from different single cell dataset were plotted with MAIT1 feature and MAIT2 feature for visualization.

Statistical analysis

Data normality and homogeneity of variance were assessed using Kolmogorov-Smirnov test and Bartlett's test, respectively. Due to the distribution and variance of human data, non-parametric statistical tests were favorably used throughout this study unless otherwise specified. Mann Whitney U test was used for two-group comparisons, and Kruskal-Wallis with post hoc Dunn's test was used for comparisons of three groups and more. Spearman's correlation efficiency was used to quantify the correlation of the ranked disease severity (from healthy as 1, to hospitalized as 4). Simple linear regression and multiple linear regression were calculated using GraphPad Prism 8. Data were transformed to meet the assumptions of linear regression when necessary. To adjust p values for multiple hypothesis testing, FDR correction was performed using the Benjamini-Hochberg procedure when appropriate. Two-tailed tests were used unless otherwise specified. A p value or FDR < 0.05 is consider statistically significant. Graphical data of quantifications presented throughout are expressed as the means $\pm$ SEMs and were plotted using Graphpad Prism 8. Other graphs in this study were generated using either the corresponding analytic packages or R package ggplot2.

Supplemental information

Mucosal-associated invariant T cell

responses differ by sex in COVID-19

Chen Yu, Sejiro Littleton, Nicholas S. Giroux, Rose Mathew, Shengli Ding, Joan Kalnitsky, Yuchen Yang, Elizabeth Petzold, Hong A. Chung, Grecia O. Rivera, Tomer Rotstein, Rui Xi, Emily R. Ko, Ephraim L. Tsalik, Gregory D. Sempowski, Thomas N. Denny, Thomas W. Burke, Micah T. McClain, Christopher W. Woods, Xiling Shen, and Daniel R. Saban
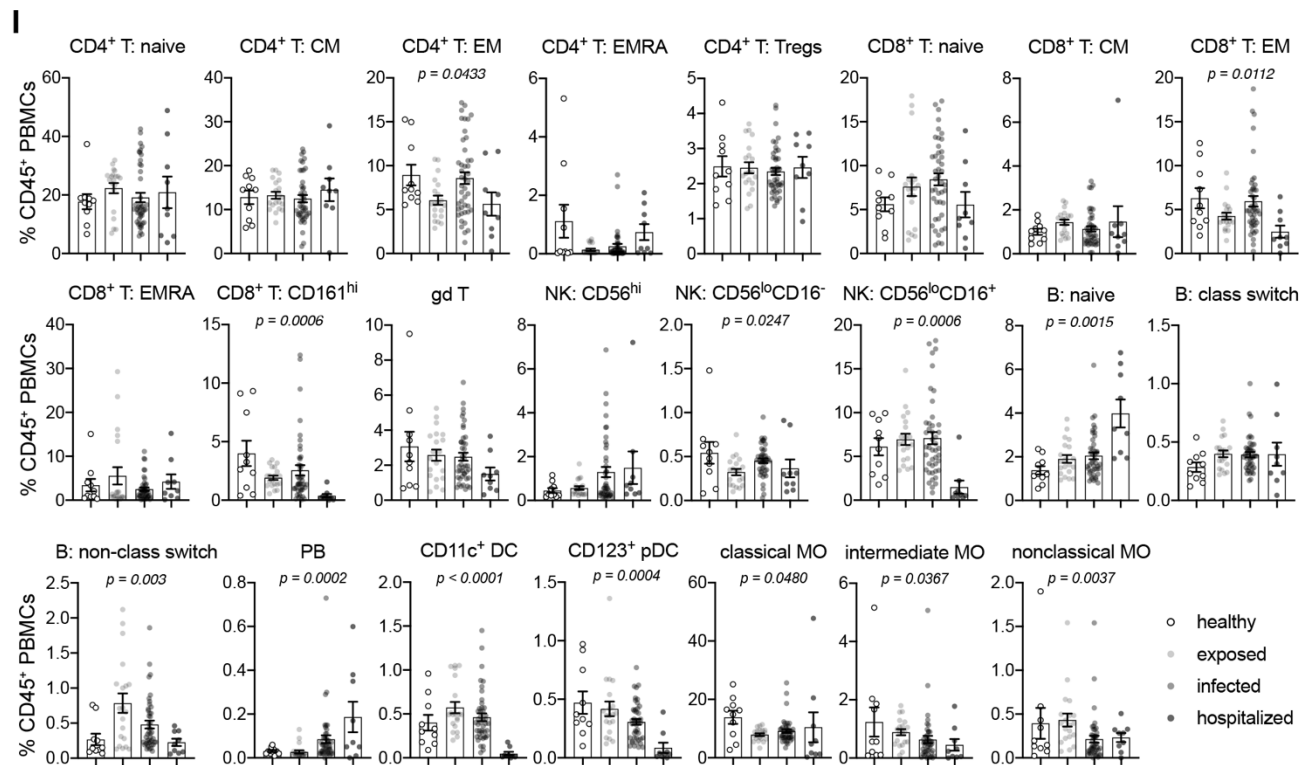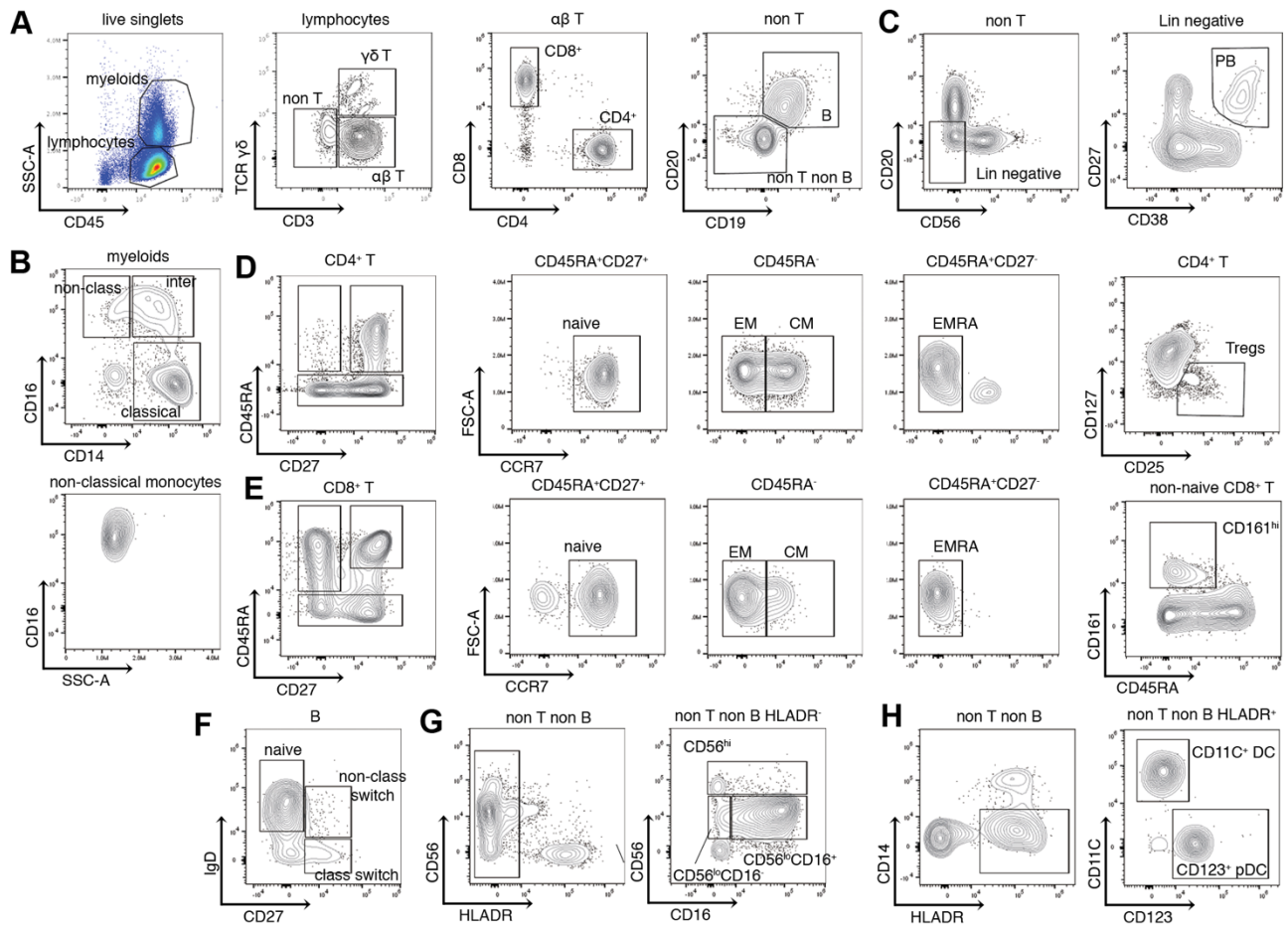
Figure S1. Manual Gating Strategy and Immune Profiling of PBMC Subsets in COVID-19, Related to Figure 1. (A-H) Gating strategy of major lymphocyte (A) and myeloid cell (B) subsets in PBMC samples, including CD4 (D) and CD8 (E) $\alpha\beta$ T cells, $\gamma\delta$ T cells (A), monocytes (B), B cells (F), plasmablasts (PB, C), NK cells (G) and dendritic cells (DC, H). (I) Frequencies of major PBMC subsets identified in A-H among healthy, exposed, infected and hospitalized groups. Significance was determined by Kruskal-Wallis test (p-values as indicated).
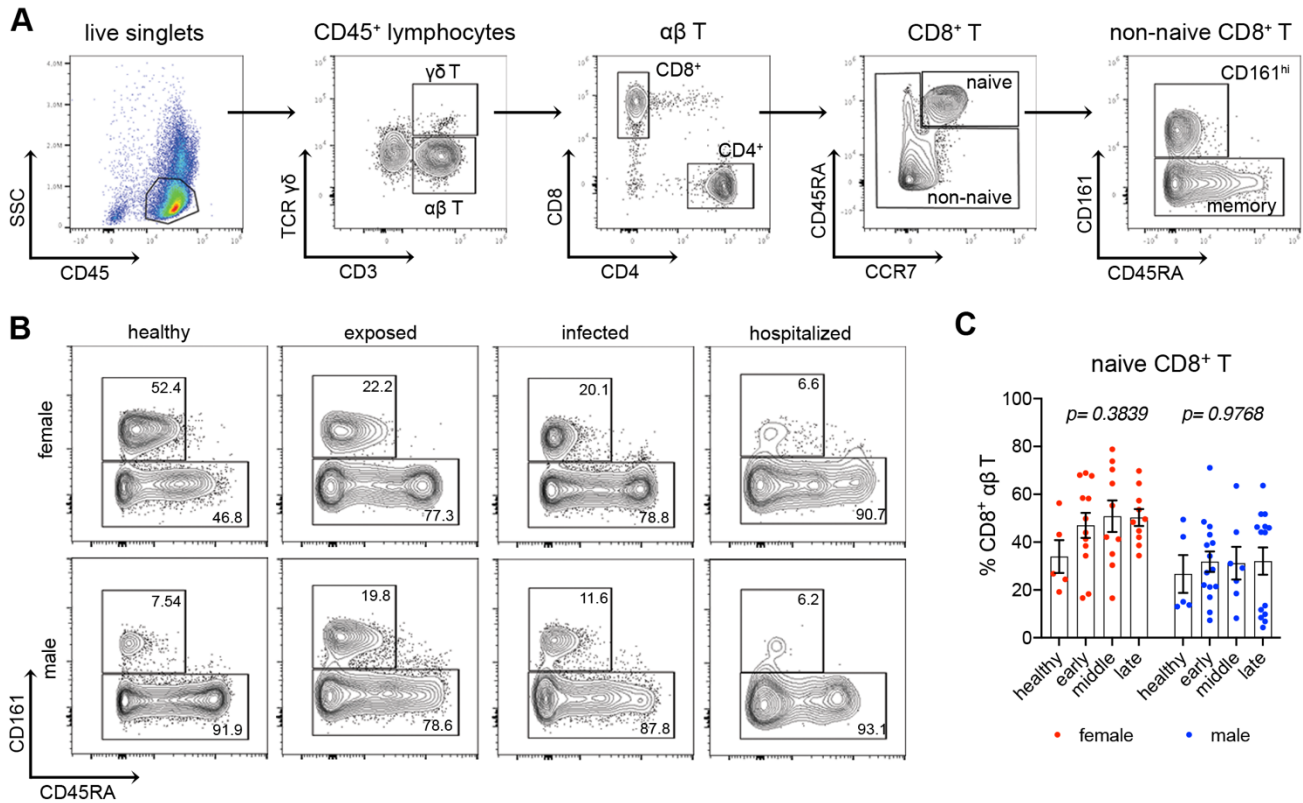
Figure S2. Sex-Specific Changes of CD8+ CD161hi and Memory T Cells in COVID-19 PBMCs analyzed by Flow Cytometry, Related to Figure 2. (A) Gating strategy of CD8+ CD161hi and memory T cells (αβ). (B) Representative flow plots of CD8+ CD161hi and memory T cells from female and male individuals with severity rank. (C) Frequencies of naïve CD8 T cells among different severity groups as indicated. Significance was calculated by Kruskal-Wallis.
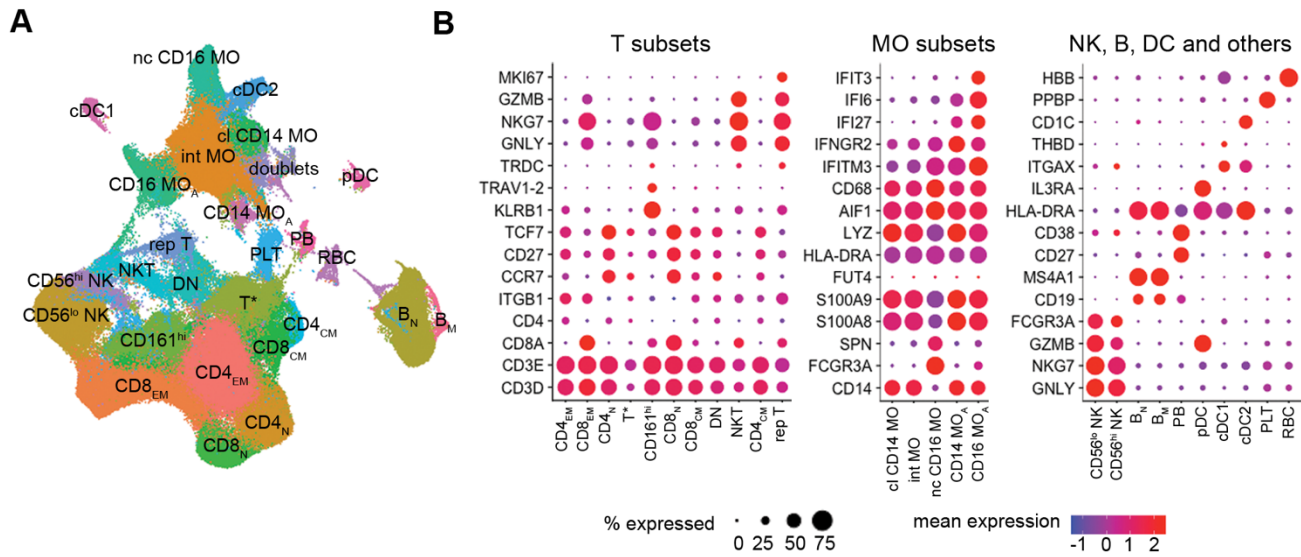
Figure S3. Characterization of Immune Subsets in COVID-19 PBMCs by scRNA-seq, Related to Figure 3. (A) High resolution clustering of PBMCs as shown in Figure 3A. (B) Expression of marker genes used to annotate the identifies of individual clusters. N, naïve; EM, effect memory; CM, central memory; DN, double negative; rep, replicating. cl, classical; int, intermediate; nc, non-classical; CD14 MO$_A$, activated CD14 monocytes; CD16 MO$_A$, activated CD16 monocytes; NK, natural killer; PB, plasmablasts; PLT, platelets; DC, dendritic cells.
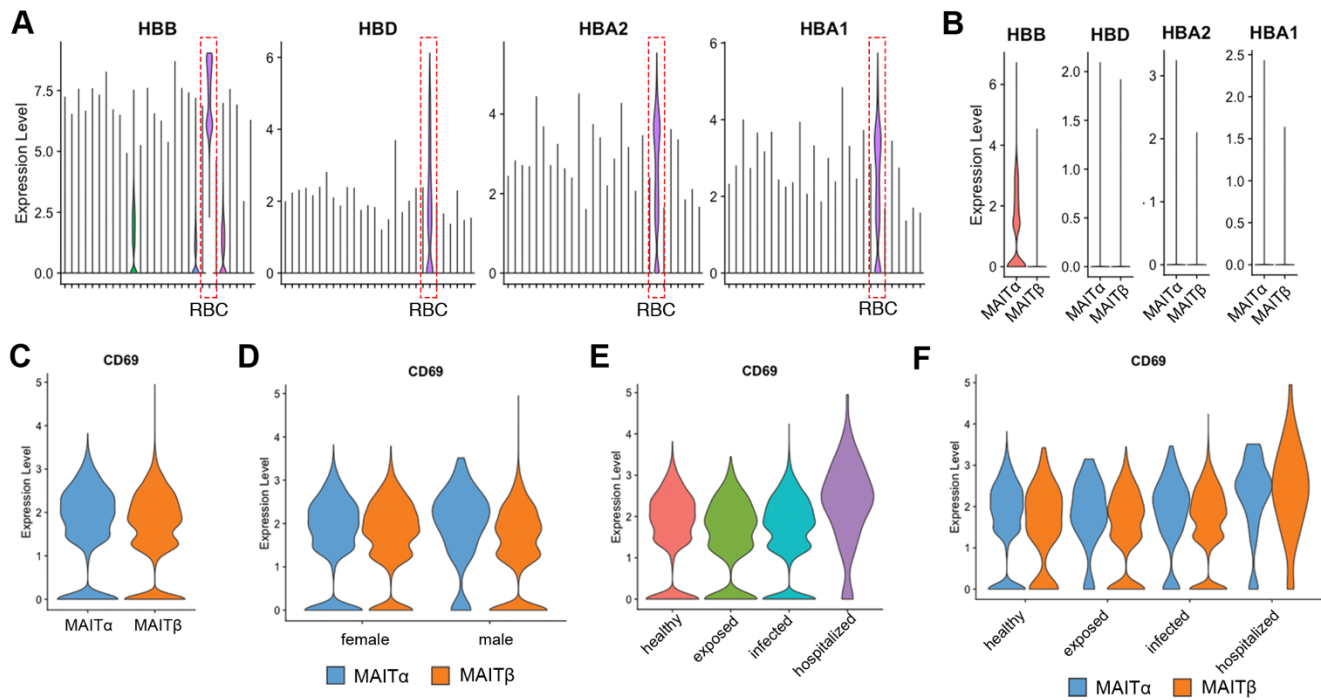
Figure S4. Expression of HBB and CD69 by Circulating MAIT Clusters in COVID-19, Related to Figure 5. (**A,B**) Expression of hemoglobin related genes (*HBB, HBD, HBA2, HBA1*) are shown by PBMC clusbters (A) and MAIT clusters (B). Red dash boxes indicates RBC cells. (C to F) Data are grouped by MAIT clusters (C), sex (D), severity rank (E) as well as clusters and severity (F).
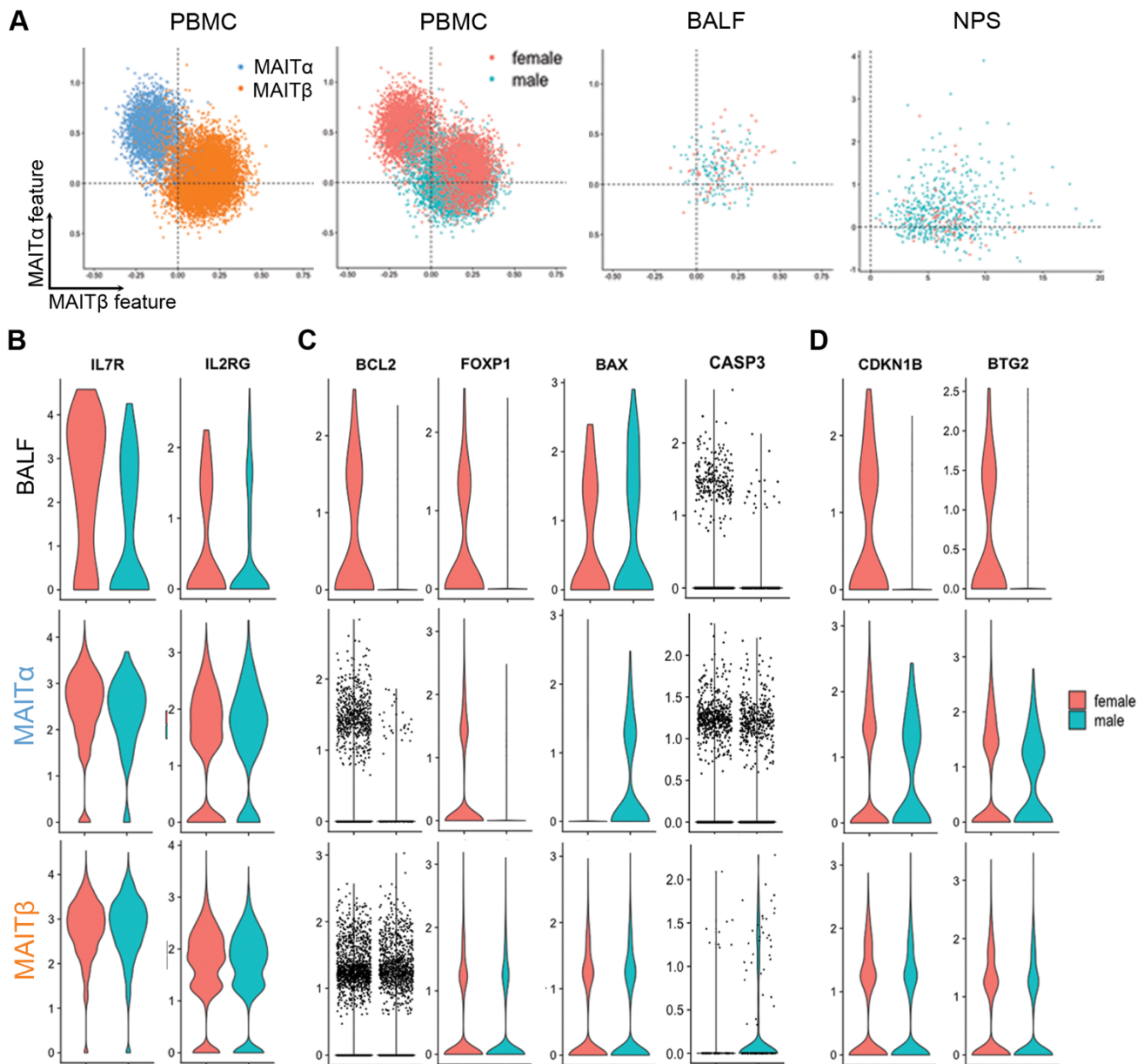
Figure S5. Comparisons of MAITα and MAITβ Features in MAIT Cells from Peripheral Blood and Airway Tissue Samples, Related to Figure 6. (A) Estimation of MAITα and MAITβ features of individual cells from PBMC and BALF dataset based on the expression of MAITα gene (y-axis) and MAITβ gene sets (x-axis). Differentially expressed genes between MAITα and MAITβ were used as two modular features, respectively. (B to D) Expression of IL7

receptor and its co-receptor genes (B), apoptosis-related genes (C), proliferation-related genes by MAIT cells from PBMC and BALF dataset (D).

Table S1. Clinical Metadata of Participants and Samples in this study, Related to Figure 1 and Table 1. Clinical data of participants in the 1st sheet 1; sample metadata in the 2nd sheet.

Table S2. List of DEGs of PBMC Clusters, Related to Figure 3. The DEGs of each PBMC cluster are listed with details of p-values (p_val), average log2 fold changes (avg_logFC), percentages of cells with the detected feature (pct.1 and pct.2), clusters and gene names.

Table S3. List of DEGs of MAIT Subsets, Related to Figure 4. The DEGs of MAITα and β are listed with details of p-values (p_val), average log2 fold changes (avg_logFC), percentages of cells with the detected feature (pct.1 and pct.2), clusters and gene names.

Table S4. List of Enriched Reactome Pathways of MAIT Subsets, Related to Figure 4. Details of the parameters provided by Reactome Pathway enrichment analysis. MAITα in the 1st sheet 1; MAITβ, the 2nd sheet.